JOURNAL OF GEOPHYSICAL RESEARCH, VOL. 96, NO. B9, PAGES 14,529–14,550, AUGUST 10, 1991

Rifting in the Northern Norwegian-Greenland Sea: Thermal Tests of Asymmetric Spreading

KATHLEEN CRANE,[1,2] EIRIK SUNDVOR,[3] ROGER BUCK,[2] AND FERNANDO MARTINEZ[4]

The analysis of heat flow, seismic, and topographic data collected in the northern Norwegian-Greenland Sea reveals an asymmetric evolution of the Eurasian and North American plates. These data are compared to predictions from three kinematic models of extension which produce asymmetry about the Knipovich Ridge: (1) uniform asymmetric pure shear, (2) lithospheric simple shear, and (3) rift/ridge jumping. The data are consistent with a range of deformation scenarios, from one ridge jump occurring at about 25 m.y. after the initiation of spreading to continuous asymmetric extension. The simple shear model can match the data only when a detachment fault dips more steeply than 45° under Svalbard. Tectonic and heat flow evidence suggests that asymmetry may have evolved from a combination of all three models. When the Mohns Ridge (propagating to the east) encountered the preexisting northward trending Spitsbergen Shear Zone, the direction of ridge propagation shifted to the north, being influenced by the abrupt change in the regional stress field at the shear zone–ridge axis intersection. As a result, the nascent Knipovich Ridge entered into and propagated along the shear zone. Consequently, formerly active shear faults became the new detachment surfaces along which new crust is minted and asymmetrically extended. The high level of deviatoric stress about the Mohns and Knipovich Ridge intersection may cause a gradual eastward migration of the Knipovich Ridge, resulting in multiple zones of magma intrusion. "Off-axial" bands of high heat flow and volcanism located along the Barents Sea and Svalbard margin, along the Yermak Plateau, and on continental Svalbard just southeast of the Yermak Plateau may be evidence for this migration. Propagation from the Nansen Ridge may have entered the same shear zone from the north, explaining the creation of the small Molloy Ridge and off-axis volcanism on the Yermak Plateau.

INTRODUCTION

In the northern Norwegian-Greenland Sea (Figure 1) the continental margins of Svalbard (Spitsbergen) and Greenland evolved first by intense shearing along the broad Spitsbergen Shear Zone (including the present-day Hornsund and Bjørnøya-Sørkapp faults (Figure 2)). Some authors suggest that transtension later developed across this shear zone, enabling the Knipovich Ridge to propagate into it from the south [*Talwani and Eldholm*, 1977; *Vogt et al.*, 1982; *Vogt*, 1986; *Crane et al.*, 1988; *Eldholm et al.*, 1990]. In their opinion the net result created ocean basins which are highly asymmetric about the present axis of spreading. In this manuscript we would like to investigate this asymmetry in the Norwegian-Greenland Sea.

Courtillot [1982], *Bonatti and Crane* [1982, 1984], and *Crane and Bonatti* [1987] suggested that when a propagating ridge intersects a preexisting shear zone, it may become deflected along or "trapped by" the highly fractured region. The oblique orientation of the shear zone relative to the direction that the propagating ridge was originally opening should result in transpression on the acute angle side of the intersection and transtension on the other side. The resultant deviatoric stress across the intersection might create asymmetric and highly oblique rifting and spreading across the evolving propagating ridge boundary (Figure 3*a*). As a result of this asymmetric pure shear extension, one flank of the ridge would extend more than the other flank [*Crane et al.*, 1988].

[1]Department of Geology and Geography, Hunter College, New York.
[2]Lamont-Doherty Geological Observatory, Palisades, New York.
[3]Seismological Observatory, University of Bergen, Norway.
[4]Hawaii Institute of Geophysics, University of Hawaii, Honolulu.

Paper number 91JB01231.
0148-0227/91/91JB-01231$05.00

Asymmetric opening could also occur if the faults within the preexisting shear zone dipped at an angle beneath the crust, making them detachment surfaces [*Wernicke*, 1981, 1985; *Wernicke and Burchfield*, 1982; *Lister et al.*, 1986; *Buck et al.*, 1988] (Figure 3*b*). A propagating rift entering the shear zone would shift its extensional mode from pure to simple shear because rifting along a detachment fault would create extension preferentially on the "lower plate" side of the fault as the lower crust and mantle lithosphere would be dragged in one direction from underneath the fracturing and extending upper crust (Figure 3*b*). If extension continued for a long time, then oceanic crust would develop asymmetrically on one side of the detachment fault. Owing to the thermal response of the asthenosphere, it is hypothesized that mantle underplating might result underneath the upper continental plate, placing ultramafic assemblages subjacent and adjacent to continental crust. In addition, upper plate margins should be more uplifted than lower plate margins and characterized by few but steeply dipping throughgoing faults on their upper crustal surfaces. Resulting from the geometry, heat flow through the crust would be highly asymmetric as well.

An additional way for asymmetric structures to develop during rifting and seafloor spreading would be a periodic shifting of the spreading center toward one direction. These shifts could occur in one or more discrete "jumps" (ridge jump shear). This rift/ridge jump model generates a net strain which is created by at least two episodes of symmetric spreading displaced laterally from one another (Figure 3*c*). Magnetic and topographic evidence of ridge jumps is recorded in the southern Norwegian-Greenland Sea [*Nunns*, 1980, 1982] but has not yet been proven or disproven in the northern Norwegian-Greenland Sea.

The purpose of this paper is to constrain the kinematic development of the Norwegian-Greenland Sea by comparing observed heat flow and topographic data with the calculated results from three models of extensional strain: (1) a purely

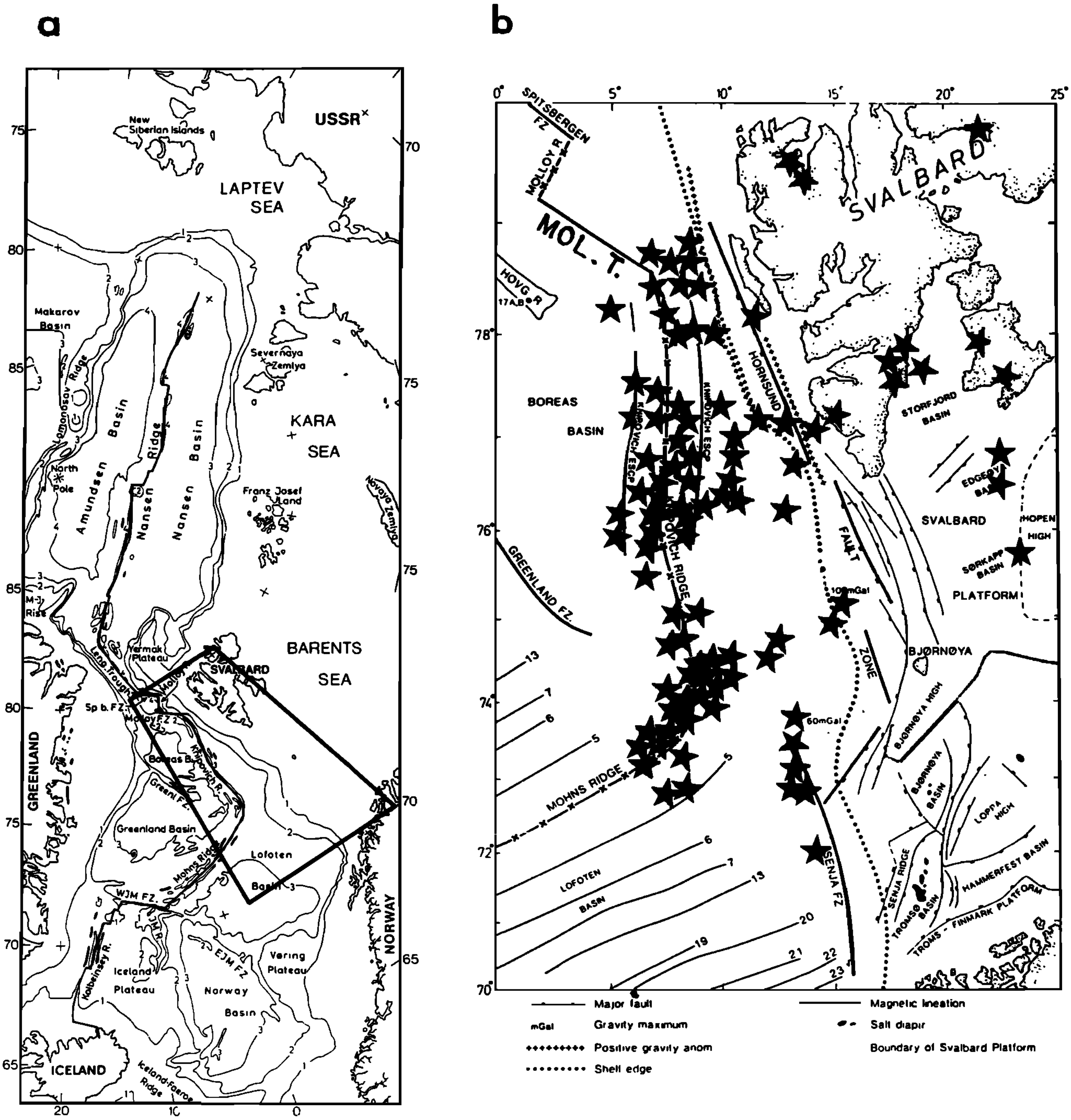

Fig. 1. (*a*) Polar stereographic map projection of the main physiographic and structural elements in the vicinity of the plate boundary north of Iceland. Selected bathymetry from *Perry et al.* [1980]: M-J Rise (Morris-Jessup Rise), WJM FZ, and EJM FZ (West and East Jan Mayen fracture zones, respectively). The enclosed region indicates the area shown in Figure 1*b* [after *Crane et al.*, 1988] (*b*) Mercator map projection of the main structural features of the Norwegian margin between 70°N and 80°N [after *Crane et al.*, 1988]. Epicenters of earthquakes between the Mohns Ridge–Knipovich Ridge intersection and the Molloy Transform fault are indicated by stars. Numbered lines represent known magnetic anomaly locations.

asymmetric spreading model, (2) a detachment model, and (3) a ridge jump model. The Norwegian-Greenland Sea (Figure 1) is a good location to test these models of extension as the position of the Knipovich Ridge (located within 100 km of the Svalbard margin) is distinctly asymmetric with respect to the geometry of the Norwegian-Greenland Sea basins. Other asymmetries occur in the basins' seismicity (with the eastern plate and margin being highly seismic (Figure 1*b*)), in the amount of uplift along the margins (the eastern margin having undergone several stages of vertical uplift and transpression along slivers of the former trace of the Spitsbergen Shear Zone (Figure 2)), and in the distribution of faults on the flanks of the spreading center (Figure 2).

Our approach is to constrain the range of two-dimensional

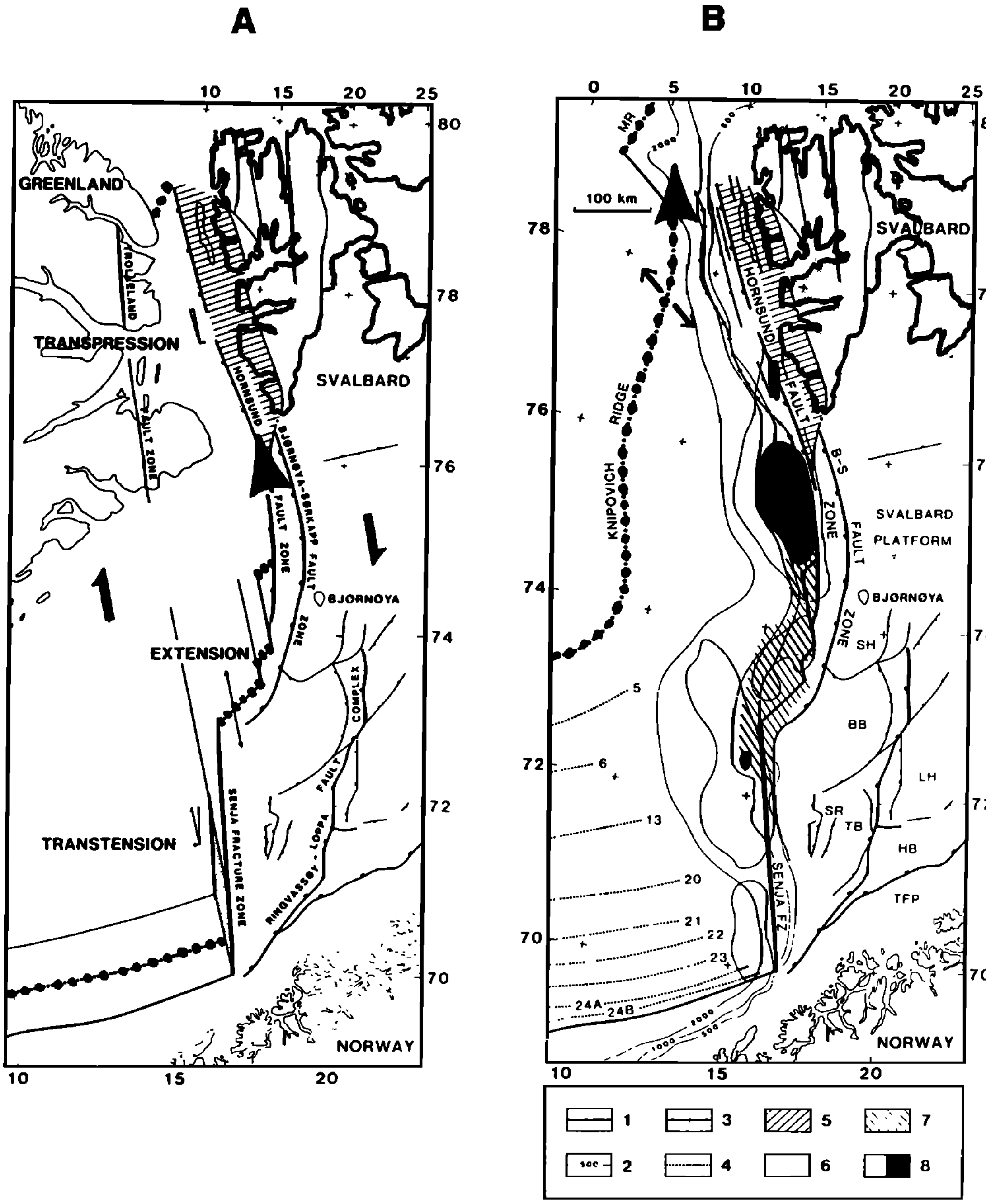

Fig. 2. Evolution of the Spitsbergen Shear Zone. (*a*) Plate tectonic setting during early opening of the Norwegian-Greenland Sea. Reconstruction to chron 23 (modified from *Eldholm et al.* [1990]) using the rotation poles of *Talwani and Eldholm* [1977]. Hachured region represents Spitsbergen Fold and Thrust Belt. Straight thin lines represent obliquely sheared crust. Dotted line represents actively spreading ridge. Large arrow indicates direction of the nascent Knipovich Ridge propagation. (*b*) Main structural features and geological provinces based on work by *Eldholm et al.* [1990]: 1, continent-ocean boundary and main structural elements; 2, bathymetry (meters); 3, limit of identified oceanic crust; 4, magnetic lineations; 5, Spitsbergen Fold and Thrust Belt; 6, Tertiary Central basin; 7, Bjørnøya Marginal High (area of early Eocene volcanism); 8, Marginal free-air gravity anomalies (>100 mGal). BB, Bjørnoya Basin; HB, Hammerfest Basin; LH, Loopa High; SH, Stappen High; SR, Senja Ridge; TB, Tromsø Basin; TFP, Troms-Finnmark Platform; B-S, Bjørnøya-Sørkapp.

kinematic deformation models which are consistent with the heat flow and topographic data. In this paper we only speculate on the mechanical causes for asymmetric basin development, but our kinematic models might give some insight into how the interaction of a propagating rift/ridge with a preexisting shear zone affects the development of a rift/spreading system.

BACKGROUND: PLATE BOUNDARY RECONNAISSANCE IN THE NORWEGIAN-GREENLAND SEA

The Mid-Atlantic Ridge can be traced into the Norwegian-Greenland Sea as the well-developed, partly sediment-covered Knipovich Ridge (Figure 1). At about 78°50'N the rift valley disappears under a thick layer of sediment.

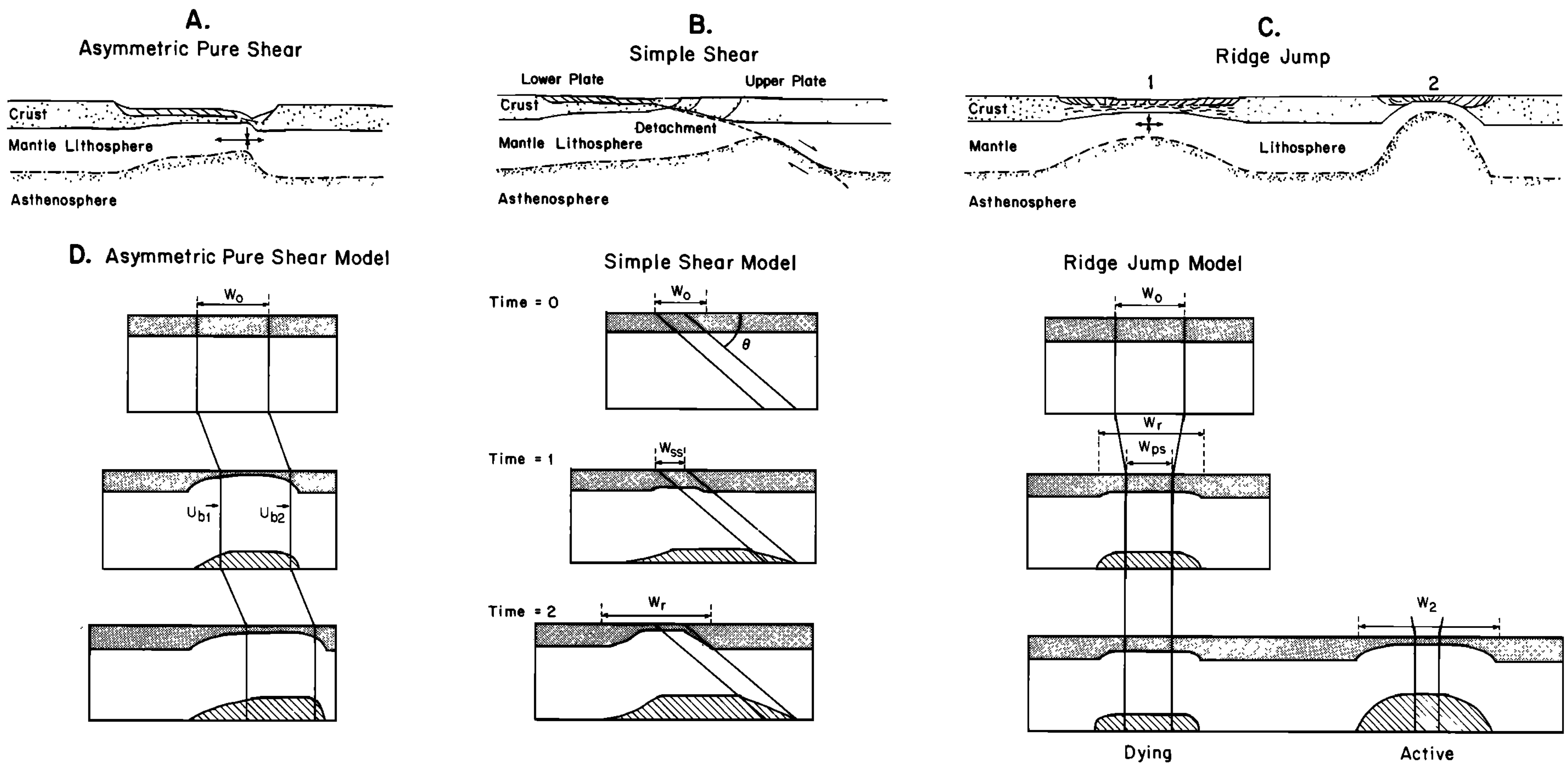

Fig. 3. Schematic geologic models depicting (*a*) asymmetric pure shear, (*b*) simple shear extension, (*c*) ridge jump extension, and (*d*) schematic diagrams of lithospheric sections showing the defining parameters of the asymmetric pure shear, the simple shear, and ridge jump models. Parameters are defined after *Buck et al.* [1988].

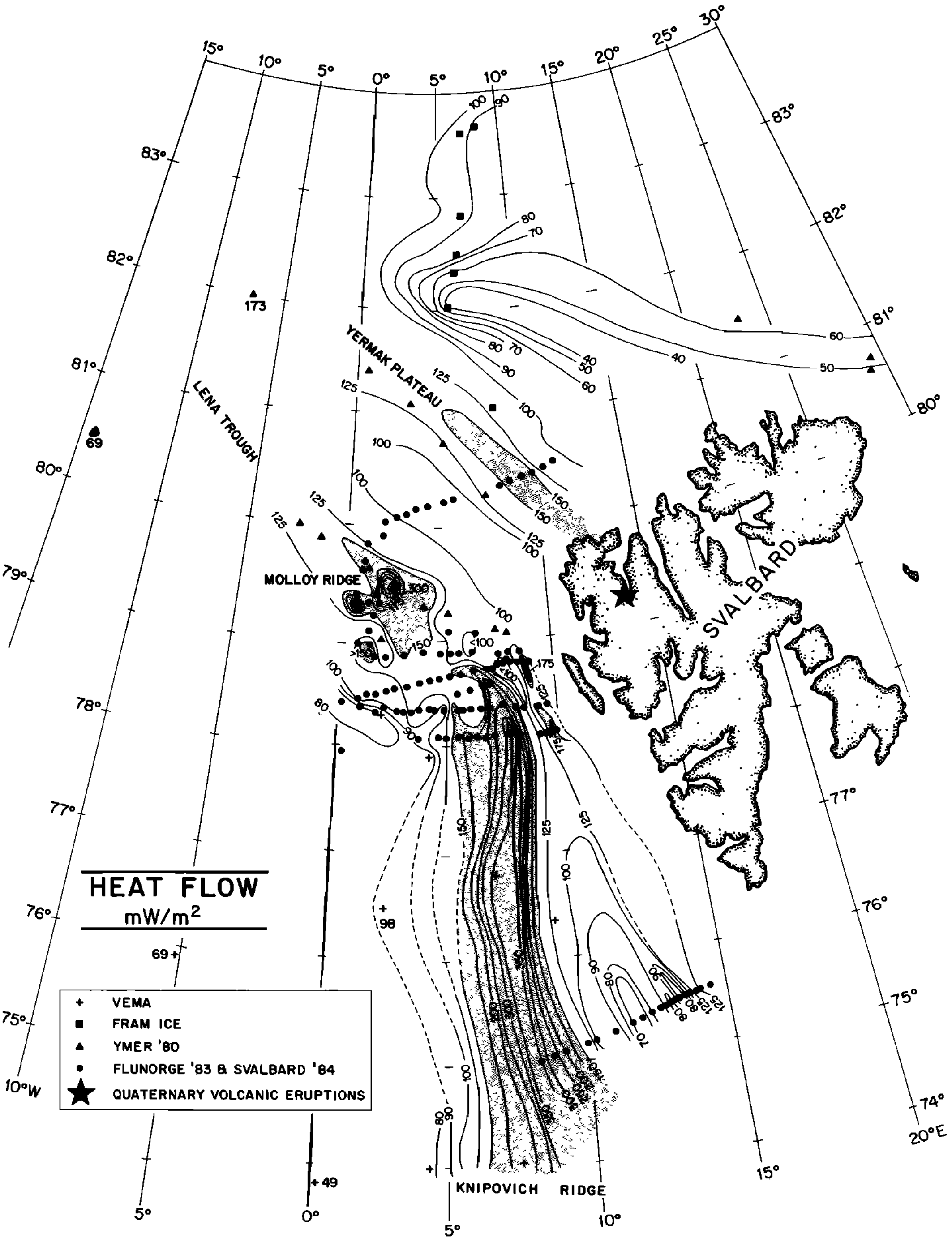

Fig. 4. Observed heat flow (in milliwatts per square meter) on the western Svalbard margin and the Yermak Plateau. Note that there is one band of relatively high heat flow (>150 mW m^{-2}) to the west and one band to the northwest of Svalbard (shaded).

Farther to the north the North American-Eurasian plate boundary appears as a structurally complex region, where northeast trending ridges interpreted as transform faults separate wide basins interpreted as oceanic crust. The plate boundary is believed to continue into the Arctic Ocean along a deep trough that was once called the Spitsbergen Fracture Zone (before at least one small spreading center was discovered within it), and its detailed structure is still not well known [*Talwani and Eldholm*, 1977; *Sundvor et al.*, 1977; *Eldholm et al.*, 1984; *Vogt*, 1986; *Thiede et al.*, 1990]. The most northerly section of this feature has been named the Lena Trough (Figure 1), which some investigators believe is an obliquely opening mid-ocean ridge [*Eldholm et al.*, 1990; *Thiede et al.*, 1990; *Perry et al.*, 1980, 1985]. Local troughs and peaks within and at right angles to the trend of the "Spitsbergen Fracture Zone" are believed to represent small pull-apart basins which have grown into tiny mid-ocean ridge segments offset by transform faults (the Molloy Ridge and Transform fault are the two best known examples (Figures 1 and 2) [*Crane et al.*, 1982; *Thiede et al.*, 1990]. To

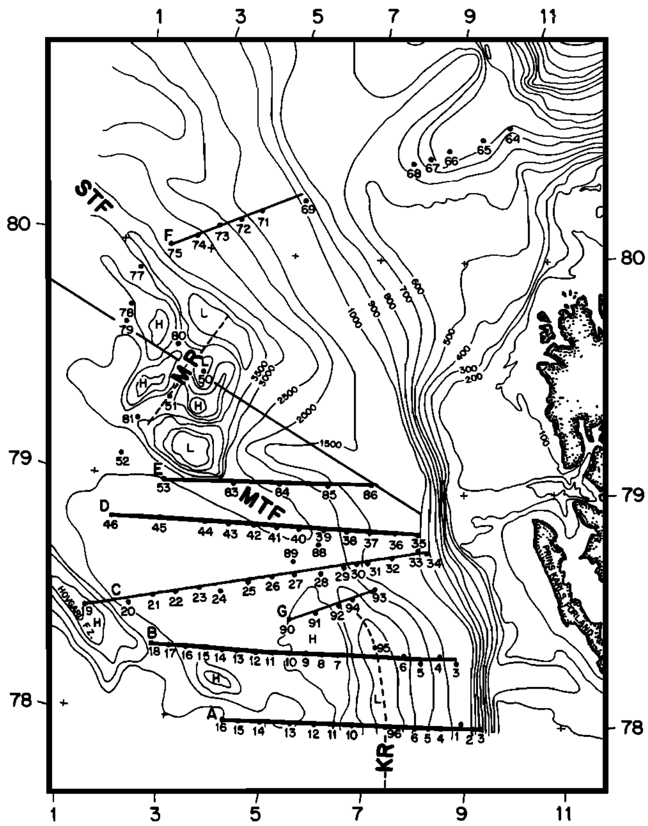

Fig. 5. Locations of heat flow lines A–G collected on Flunorge, 1983, and Svalbard, 1984. MR, Molloy Ridge; STF, Spitsbergen Transform fault; MTF, Molloy Transform fault; and KR, axis of the Knipovich Ridge. Bathymetric contours in meters.

the southeast of this region lies the Knipovich Ridge (almost a linear extension of the Lena Trough and the Molloy Ridge-Transform fault system (Figure 1)).

The complexity of the plate boundary in the Norwegian-Greenland Sea reflects the complex opening history in this area. Seafloor spreading in the Norwegian Sea and the Arctic Ocean started at approximately chron 25–24 [*Talwani and Eldholm*, 1977; *Vogt and Avery*, 1974], that is, about 66–57 Ma on the *LaBrecque et al.* [1977] time scale (Figure 2). The relative motion between Svalbard and Greenland was approximately northwest-southeast from the Mohns Ridge with no crustal extension in the Greenland Sea. A regional continental transform fault system acted as the plate boundary between the incipient Norwegian Sea and the Arctic Ocean (the ancient Spitsbergen Shear Zone) [*Talwani and Eldholm*, 1977] (Figure 2).

Evidence for Rift Propagation

The initiation of seafloor spreading in the southern part of the Norwegian-Greenland Sea was first revealed by the mid-1970s aeromagnetic surveys [*Vogt et al.*, 1978, 1981; *Myhre et al.*, 1982; J. D. Phillips et al., Naval Research Laboratory, Washington, D. C., Aeromagnetic studies of the Greenland/Norwegian Sea and Arctic Ocean, unpublished manuscript, 1982]. *Talwani and Eldholm* [1977] proposed that at about chron 13 (36 Ma) the pole of rotation changed, increasing the east-west component of opening, starting seafloor spreading in the northern Norwegian-Greenland Sea along the Knipovich Ridge. However, *Vogt et al.* [1982] and *Kovachs and Vogt* [1982] suggested that magnetic anomalies older than chron 13 exist in the western Boreas Basin. This conflicts with the earlier conclusion by *Talwani and Eldholm* [1977] that prior to 36 Ma there was only shear between the Greenland-Svalbard margin.

On the basis of the analysis of heat flow, *Crane et al.* [1988] suggested opening ages of 60 Ma at a latitude of 75°N and 30–40 Ma at a latitude of 78°N. According to their calculations, seafloor opening propagated northward at a rate of 1° 10 m.y.$^{-1}$, yielding spreading rates of 4.5 mm/yr at 75°N, dropping to between 1.5 and 3.1 mm yr^{-1} at the intersection with the Molloy Transform fault (78°N). *Crane et al.* [1988] also suggested that the North American plate is growing at a rate of 1.5 times as fast as the Eurasian plate across the Knipovich Ridge. In contrast, *Vogt* [1986], using North American–Eurasian plate kinematic models, computed the half spreading rate across the Knipovich Ridge to be 7.5 mm yr^{-1}.

The structural geometry also supports the hypothesis of ridge propagation. The best examples are the truncation of two "fracture zone" ridges south of and parallel to the Lena Trough of the Spitsbergen Shear Zone: the Hovgård Ridge and the Greenland Fracture Zone Ridge, which cut across the Norwegian-Greenland Sea (Figure 1*b*). These are presumed to be paleofault blocks (part of the greater Spitsbergen Shear Zone) that were rafted away and deactivated from the shear zone by the propagation of the Knipovich Ridge northward [*Crane et al.*, 1988]. Furthermore, *Myhre et al.* [1982], *Myhre* [1984], *Myhre and Eldholm* [1987], and *Eldholm et al.* [1987] believe that the Hovgård Ridge is a piece of continental crust slivered off of the eastern continental margin during episodes of transtension and northward rift propagation.

Complicating the northward propagation scenario are the Molloy Ridge and the Lena trough. *Eldholm et al.* [1990] suggest that the Lena Trough is an obliquely opening remnant of the Spitsbergen Shear Zone, much the same as the Knipovich Ridge only more poorly mapped. *Crane et al.* [1982] suggested that sections of the northern Spitsbergen Shear Zone (the Lena Trough) had been invaded by rift propagation southward from the Nansen Ridge. They inferred that the Molloy Ridge might also have developed before the northern Knipovich Ridge because the Molloy Ridge was farther away from the Svalbard continental margin, suggesting more developed spreading.

If propagation did proceed from the Nansen ridge south into the Spitsbergen Shear Zone, then much of the Lena Trough may be broken up into pull-apart basins and small offset transform faults. If propagation is only progressing from south to north, then the Lena Trough may be a region primarily under shear. In either case, spreading on the Knipovich Ridge would have originated in the south. Thus rifting and spreading should be structurally and thermally advanced in the south compared to the northern part of the ridge axis. Consequently, one should be able to map changing fault structures and geophysical parameters from south to north, corresponding to a near-extensional regime in the south to a near-shear regime in the north, respectively. The degree to which different sections of this ancient shear remain a transform fault, a region of transtension, or a fully fledged spreading center is not well known as bathymetric

TABLE 1. Heat Flow Data From Svalbard 1984

Station	Latitude, N	Longitude, E	Depth, m	Number of Thermistors	Penetration, m	Gradient mK m^{-1}	K,* W m^{-1} K^{-1}	Heat Flow, m W m^{-2}
				Transect B				
1	78°18.13′	9°10.83′	883	5	4.6	NL		
2	78°18.13′	9°11.50′	879	5	4.6	NL		
3	78°17.27′	8°50.42′	1390	4	4.6	82 ± 1	1.221	100 ± 1
4	78°18.00′	8°29.82′	1870	5	4.6	92 ± 4	1.096	101 ± 4
5	78°16.92′	8°06.52′	2329	4	4.6	113 ± 4	1.10E	124 ± 4
6	78°18.26′	7°47.16′	2674	4	4.6	227 ± 7	1.10E	250 ± 8
95	78°20.48′	7°11.21′	3288	5	4.6	239 ± 3	1.23V	294 ± 4
7	78°17.80′	6°25.06′	1834	3	4.6	122 ± 4	1.11F	135 ± 4
8	78°18.05′	6°07.01′	1825	3	4.6	143 ± 4	1.11F	159 ± 4
9	78°18.14′	5°45.27′	1670	4	4.6	113 ± 2	1.11F	125 ± 2
10	78°18.67′	5°25.56′	1928	4	4.6	161 ± 2	1.11F	179 ± 2
11	78°18.34′	5°04.53′	1947	3	4.6	73 ± 3	1.11F	81 ± 3
12	78°18.05′	4°45.11′	2245	3	4.6	97 ± 2	1.11F	108 ± 2
13A	78°18.23′	4°22.10′	2223	4	4.6	106 ± 2	1.11F	117 ± 2
13B	78°18.23′	4°21.67′	2217	4	4.6	104 ± 2	1.11F	115 ± 2
14	78°18.45′	4°02.09′	2280	5	4.6	93 ± 5	1.11F	103 ± 6
15	78°18.41′	3°40.20′	2438	5	4.6	133 ± 5	1.11F	147 ± 6
16	78°17.99′	3°16.80′	2546	3	4.6	80 ± 1	1.11F	89 ± 1
17	78°18.22′	2°56.01′	2846	4	4.6	107 ± 5	1.11F	119 ± 6
18	78°18.05′	2°35.58′	2566	3	4.6	63 ± 2	1.11F	70 ± 2
				Transect C				
34	78°44.95′	8°10.88′	897	5	4.6	65 ± 4	1.00Y	65 ± 4
33	78°45.55′	8°01.02′	978	5	4.6	122 ± 4	1.00Y	122 ± 4
32	78°43.81′	7°28.82′	1146	4	4.6	101 ± 5	1.00Y	101 ± 5
31	78°42.17′	6°58.54′	1412	4	4.6	114 ± 1	1.00Y	114 ± 1
30	78°41.83′	6°44.36′	1560	4	4.6	118 ± 3	1.00Y	118 ± 3
29	78°40.96′	6°29.40′	1740	5	4.6	118 ± 2	1.00Y	118 ± 2
28	78°39.27′	6°01.72′	2455	4	4.6	NL		
27	78°38.10′	5°29.31′	2340	4	4.6	145 ± 6	1.06E	154 ± 6
26	78°37.18′	5°01.68′	2332	4	4.6	147 ± 13	1.064	156 ± 14
25	78°35.51′	4°29.75′	2369	5	4.6	130 ± 2	1.06E	138 ± 2
24	78°33.05′	3°56.29′	2325	4	4.6	121 ± 5	1.06E	128 ± 5
23	78°33.29′	3°28.37′	2456	5	4.6	122 ± 6	1.06E	129 ± 6
22	78°31.80′	2°59.65′	2500	5	4.6	104 ± 6	1.06E	110 ± 6
21	78°30.52′	2°30.29′	2386	5	4.6	104 ± 3	1.06E	110 ± 3
20	78°28.15′	2°00.06′	2566	5	4.6	102 ± 5	1.06E	108 ± 5
19A	78°26.04′	1°07.67′	1273	3	4.6	85 ± 5	1.30V	111 ± 6
19B	78°26.06′	1°07.10′	1267	3	4.6	82 ± 1	1.30V	107 ± 1

NL, nonlinear gradient.

*E, conductivity estimated from nearby corings; F, conductivity estimated from Flunorge 1983 survey; Y, conductivity estimated from *Crane et al.* [1982]; and V, conductivity estimated from *Langseth and Zielinski* [1974].

and geophysical data are almost nonexistent in the northernmost regions due to year-round ice cover.

Asymmetries Across the Knipovich Ridge

Geophysical and spreading rate asymmetries within the Norwegian-Greenland Sea have been widely reported [*Johnson et al.*, 1972; *Vogt et al.*, 1982; *Kovacs and Vogt*, 1982; *Nunns and Peacock*, 1983; *Nunns*, 1983]. *Stein et al.* [1977] proposed that asymmetry could develop when one of the two developing plates is traveling faster with respect to the deeper mantle. Thus more crust will be accreted to the slower plate. *Minster and Jordan* [1978] and *Morgan* [1981] have suggested that the North American plate has moved much more rapidly than the quasi-stationary Eurasian plate. This would seem to refute the *Stein et al.* [1977] hypothesis, because crust is apparently accreting more rapidly on the faster North American side [*Vogt et al.*, 1982].

Tectonic asymmetries across the Norwegian-Greenland Sea reached their height during the Tertiary when Svalbard was subject to strong tectonic deformation along 300 km in a NNW–SSE direction along the western margin [*Birkenmajer*, 1981]. The deformation was in the form of strong folding and low-angle thrusting in a zone 10–20 km wide. The thrusting was generally to the north or northeast. Up to three to five thrust sheets were formed which overrode one another for distances of 1–4 km. The age of the onset of folding is thought to be post-lower Paleocene (58 Ma). Compression continued either up to pre- or post-Oligocene (23–37 Ma). The first stage involved a forceful push from the southwest of the western block, which was thrust over the southwest margin of the central depression of Spitsbergen. At the same time there was a translation of 30 km or more to the NNW along the shear zone. This compression is much more pronounced on Svalbard than on the equivalent margin of northern Greenland.

Seismic asymmetry is very pronounced across the Knipovich Ridge. Even today there is a region of anomalous seismic activity extending from Spitsbergen west to the Knipovich Ridge (Figure 1*b*). In contrast, the western Boreas Basin is nearly aseismic. Unfortunately, to date,

TABLE 2. Heat Flow Data From Svalbard 1984

Station	Latitude, N	Longitude, E	Depth, m	Number of Thermistors	Penetration, m	Gradient, mK m^{-1}	K,* W m^{-1} K^{-1}	Heat Flow, m W m^{-2}
Transect D								
35	78°50.00′	8°01.43′	1003	6	4.6	85 ± 3	1.00Y	85 ± 3
36	78°49.96′	7°30.93′	1142	6	4.6	107 ± 4	1.00Y	107 ± 4
37	78°49.97′	7°00.53′	1426	4	4.6	116 ± 2	1.00Y	116 ± 2
38	78°50.14′	6°29.48′	1960	5	4.6	117 ± 1	1.00Y	117 ± 1
39	78°50.28′	5°58.52′	2454	4	4.6	82 ± 8	1.06E	87 ± 8
40	78°49.93′	5°30.08′	2578	4	4.6	88 ± 10	1.06E	93 ± 11
41	78°49.92′	5°00.77′	2667	4	4.6	121 ± 44	1.06E	128 ± 4
42	78°49.67′	4°29.93′	2405	4	4.6	102 ± 12	1.20E	117 ± 13
43	78°50.06′	3°59.21′	2312	5	4.6	104 ± 6	1.20E	125 ± 7
44	78°50.14′	3°28.70′	2310	4	4.6	123 ± 3	1.199	148 ± 4
45	78°50.07′	2°28.69′	2492	4	4.6	81 ± 13	1.20E	97 ± 16
46	78°49.51′	1°27.84′	2507	3	4.6	85 ± 10	1.20E	102 ± 12
Transect E								
86	79°01.97′	7°00.02′	1290	5	4.6	102 ± 3	1.007	103 ± 3
85	79°01.18′	5°58.10′	1685	4	4.6	98 ± 4	1.01E	99 ± 4
84	79°01.46′	5°01.81′	2184	5	4.6	114 ± 1	1.01E	115 ± 1
83	79°00.38′	3°59.70′	2730	5	4.6	114 ± 2	1.36E	155 ± 3
53	78°59.86′	2°29.15′	2429	4	4.6	79 ± 1	1.357	107 ± 1
Transect F								
69	80°13.91′	5°08.36′	800	3	4.6	70 ± 3	1.02E	71 ± 3
70	80°11.73′	4°36.18′	1070		NP			
71	80°10.46′	4°07.81′	1303	5	4.6	83 ± 4	1.02E	85 ± 4
72	80°08.22′	3°39.21′	1727	5	4.6	86 ± 2	1.02E	88 ± 2
73	80°06.15′	3°06.30′	2078	5	4.6	88 ± 2	1.02E	90 ± 2
74	80°03.06′	2°39.93′	2549	5	4.6	99 ± 3	1.02E	101 ± 3
75	79°59.93′	2°01.17′	2750	4	4.6	103 ± 2	1.018	105 ± 2
Transect G								
93	78°35.42′	7°07.07′	1735	5	4.6	91 ± 4	1.00Y	91 ± 4
94	78°32.38′	6°37.86′	2774	5	4.6	197 ± 2	1.00Y	197 ± 2
92	78°30.95′	6°22.33′	2303	4	4.6	125 ± 1	1.00Y	125 ± 1
91	78°28.35′	5°55.03′	1905	5	4.6	131 ± 2	1.06E	139 ± 2
90	78°26.57′	5°24.26′	1874	5	4.6	129 ± 2	1.06E	137 ± 2
Molloy Ridge								
50	79°28.67′	3°04.62′	3620	4	4.6	291 ± 5	0.98E	285 ± 5
51	79°21.55′	2°23.77′	3336	5	4.6	204 ± 2	0.98E	200 ± 2
80	79°34.43′	2°27.69′	2890	5	4.6	280 ± 7	0.98E	274 ± 7
81	79°15.14′	1°45.36′	3430	5	4.6	147 ± 2	0.977	144 ± 2
77	79°52.98′	1°23.49′	2969	4	4.6	121 ± 3	1.02E	123 ± 3
78	79°43.33′	1°19.77′	2570	5	4.6	158 ± 3	1.02E	161 ± 3
79	79°39.15′	1°13.11′	2635	5	4.6	163 ± 3	1.02E	166 ± 3
52	79°05.70′	1°30.32′	2604	5	4.6	98 ± 5	1.36E	133 ± 6
Yermak Plateau								
64	80°32.78′	10°01.25′	813	5	4.6	90 ± 5	1.16Y	104 ± 6
65	80°28.87′	9°28.10′	880	4	4.6	98 ± 1	1.16Y	114 ± 1
66	80°26.62′	8°49.29′	840	5	4.6	113 ± 2	1.16Y	131 ± 2
67	80°24.73′	8°14.86′	813	5	4.6	119 ± 5	1.16Y	138 ± 6
68	80°22.15′	7°42.82′	688	5	4.6	108 ± 5	1.16Y	125 ± 6
Knipovich Ridge								
96	78°00.40′	7°26.34′	3530	5	4.6	245 ± 3	1.23V	301 ± 4

*E, conductivity estimated from nearby corings; Y, conductivity estimated from *Crane et al.* [1982]; F, conductivity estimated from Flunorge 1983 survey; V, conductivity estimated from *Langseth and Zielinski* [1974].

very few focal depths have been established. However, first motions have been determined for several earthquakes on Svalbard [*Chan and Mitchell*, 1985]. They indicate sinistral strike-slip motion on ESE striking faults, which are fairly oblique to all of the known major faults in the region. This seismic asymmetry across the Knipovich Ridge suggests widespread tectonic disturbances on the Eurasian plate.

The flanks of the Knipovich Ridge are also structurally asymmetric. The axis is bounded near Svalbard by an eastern margin which is narrow, broken by only a few steep faults of which the Hornsund fault is the most dominant (Figures 2 and 6). The western flank is broken by numerous normal faults (Figure 6). In addition, a glance at Figures 4–6 reveals that surface heat flow is also very asymmetric across the Knipovich Ridge with the peak of the heat flow offset to the east of the axis followed by a rapid cooling on the eastern flank.

This asymmetry is the focus of much of the upcoming discussion in which 80 new heat flow stations (Figures 4–6) are used to constrain the thermal/age/spreading rate evolu-

TABLE 3. Heat Flow Data From Vema Expeditions and Ymer 80

Station	Latitude, °N	Longitude	Depth, m	Number of Thermistors	Penetration, m	Gradient, mK m^{-1}	Conductivity, W m^{-1} K^{-1}	Heat Flow, mW m^{-2}
				Vema				
143	75°56′	5°07′W	3129	···	···	70	0.98	69*
144	73°48′	0°06′E	2964	···	···	48	1.01	49*
108	76°25′	2°15′E	3183	···	···	97	1.14	98*
109	77°52′	4°08′E	3075	···	···	89	1.12	99*
110	78°19′	2°00′E	2006	···	···	63	1.30	81*
111	76°17′	9°07′E	2243	···	···	110	1.08	118*
112	76°41′	6°52′E	2413	···	···	>470	0.98	461*
				Ymer				
2	76°26.75′	01°27.17′E	3170	4	7.63	137	0.99 ± 0.049	137 ± 5
3	79°15.65′	00°47.31′E	2952	3	12.2	204	1.12 ± 0.087	229 ± 18
4	80°28.99′	14°23.62′W	325	3	3.94	66.7	1.04 ± 0.03	69 ± 2
6	82°00.14′	07°05.00′W	3350	3	5.75	162	1.065 ± 0.08	173 ± 12
8	81°24.20′	00°53.81′E	1596	5	8.10	131	0.990 ± 0.08	130 ± 10
9	81°06.46′	03°16.32′E	820	4	7.18	122.5	0.083 + 0.16Z ± 0.08	343 ± 10
10	80°47.18′	05°06.42′E	682	5	7.58	96.5	0.975 + 0.12Z ± 0.08	212 ± 8
11	79°59.80′	02°21.78′W	2680	3	3.01	104	1.04 + 0.99Z ± 0.08	442 ± 8
12	79°51.15′	01°10.48′W	2734	5	7.38	101.7	0.808 + 0.19Z ± 0.07	147 ± 7
13	79°19.53′	04°03.02′E	2910	5	7.12	180.6	0.9980 ± 0.09	179 ± 16
14	79°15.86′	05°11.33′E	1750	4	8.12	135.2	0.890 ± 0.1	120 ± 14
15	78°45.00′	07°29.14′E	1154	4	7.7	117.5	1.00 ± 0.07	118 ± 4
16	80°16.44′	07°05.08′E	560	4	5.6	96.6	1.14 ± 0.11	110 ± 11
17	81°25.14′	23°17.89′E	502	5	7.63	54.5	1.12 ± 0.158	61 ± 9
18	81°33.00′	29°22.52′E	1512	5	7.70	38.5	0.69 + 0.35Z ± 0.09	109 ± 65
20	80°41.31′	29°27.63′E	462	5	6.1	58.7	0.96 ± 0.04	57 ± 2

Dots, Information unknown. Vema from *Langseth and Zielinski* [1974] and Ymer 80 from *Crane et al.* [1982]. Z indicates depth down to core.

*Unknown heat flow uncertainty.

tionary models for the Knipovich Ridge. In the following sections we numerically test the asymmetric pure shear, simple shear, and ridge jump extension models against the collected heat flow and topographic data sets to see which could explain the onset of apparent asymmetric rifting from the Knipovich Ridge.

HEAT FLOW

One way to assess the mode of asymmetric rifting in the Norwegian-Greenland Sea is to analyze heat flow from the plateaus, ridges, and basins in this region. *Crane et al.* [1982] made the first attempt at a regional thermal map. They showed that the northern part of the "Spitsbergen Fracture Zone" is probably broken into at least three segments separated by small pull-apart basins. Heat flow was discovered to be abnormally high on the northwest segment of the Yermak Plateau adjacent to the "fracture zone" (Figure 4). In the fall of 1983 a joint Norwegian, French, and American expedition took a total of 39 heat flow measurements along two east-west lines from the continental shelf of Svalbard across the Knipovich Ridge to the Hovgård Fracture Zone (78°N and 75.2°N [*Crane et al.*, 1988], Figure 4). These data indicated a significant heat source beneath the Molloy Ridge/Transform region and on the shallow Yermak Plateau. In addition, as mentioned earlier, it was discovered that heat flow across the Knipovich Ridge is very asymmetric.

Crane et al. [1988] attempted to match the 1983 heat flow data, corrected for sedimentation, with simple McKenzie-type (pure shear) models for the age-dependent cooling of oceanic crust [*McKenzie*, 1978]. The southern transect at 75°N fit the model relatively well, yet the farther north one looked, the worse the fit between the observed and the predicted data along the eastern flank of the spreading center. Figures 4 and 5 and Tables 1–4 display the locations of the additional heat flow data collected in 1984 combined with the earlier data sets. These new data are used in the following discussion to constrain the above mentioned extension models.

To calculate heat flow accurately, the thermal effects of sedimentation are taken into account. To this end, all seismic profiles along our heat flow transects are analyzed, and the best estimates for sediment type and thickness are determined based on sound velocity profiles and core samples taken in the region.

Sedimentation rates in this region are extremely high. *Myhre and Eldholm* [1987] and *Myhre* [1984] estimate that prior to the mid-Miocene the rate was aproximately 100 mm.y. Since the Miocene (during the last 5 m.y.) the rates have increased to more than 300 mm.y. Two acoustic reflectors in the sediment (horizons A and B) which presumably represent these rate changes have been mapped by *Faleide et al.* [1984]. They suggest that horizon B represents the base of the upper Paleocene unconformity. It was about this time that block faulting was initiated adjacent to Svalbard. Between the A and B horizons there is evidence of initial progradation of local unconformities. *Faleide et al.* [1984] interpreted these unconformities as a resultant of sporadic tectonic activity near the present ocean/continental crust boundary. The A reflector is probably related to the drop in sea level in mid-Oligocene time.

Myhre et al. [1982] proposed that all of the sediment north of 76°N and seaward of the Hornsund fault zone was deposited since the mid-Oligocene. They designate three horizons (the first, second, and third horizons), from which they date the base of the second horizon as ~5.5 Ma (Figure 6).

TABLE 4. Heat Flow Data From Flunorge 1983

Station	Latitude, N	Longitude, E	Depth, m	Number of Therm.	Penetration, m	Gradient, mK m^{-1}	Conductivity, W m^{-1} K^{-1}	Heat Flow, mW m^{-2}
1	78°01.50′	08°54.05′	1327	3	3.2	118 ± 6	0.97	114 ± 5
2	78°00.30′	09°09.24′	1000	7	4.7	99 ± 5	1.31 ± 0.29	130 ± 36
3	78°00.42′	09°19.70′	733	4	4.2	109 ± 14	1.61	175 ± 22
4	77°59.98′	08°29.31′	1780	6	4.6	112 ± 6	0.97	109 ± 6
5	78°00.48′	08°16.03′	2089	6	4.6	185 ± 3	0.97	179 ± 3
6A	77°59.79′	07°57.10′	2560	4	3.9	460 ± 4	0.97	446 ± 4
6B	77°59.96′	07°57.54′	2560	4	3.9	306 ± 3	0.97	297 ± 3
8	78°01.08′	09°18.49′	727	7	8.0	79 ± 1	1.575 + 0.025Z	132 ± 3
10	77°59.70′	06°45.07′	2396	3	3.9	210 ± 1	1.11	233 ± 1
11	78°00.21′	06°22.42′	2037	3	3.9	162 ± 15	1.11	180 ± 17
12	78°00.19′	06°00.12′	2350	3	3.9	142 ± 5	1.11	158 ± 6
13	78°00.07′	05°30.76′	2570	3	3.9	160 ± 5	1.11	176 ± 6
14	78°00.53′	04°55.61′	2863	7	4.0	110 ± 4	1.11	121 ± 4
15	77°59.76′	04°30.03′	2745	7	4.3	91 ± 2	1.008 + 0.7Z	108 ± 2
16	78°00.00′	04°00.13′	3046	3	3.9	89 ± 1	1.11	98 ± 1
17A	78°20.28′	01°27.71′	1375	3	3.9	62 ± 10	1.29	80 ± 13
17B	78°20.28′	01°27.60′	1375	3	3.9	59 ± 10	1.29	76 ± 13
18	75°26.50′	14°14.20′	620	6	4.7	14 ± 6	1.165 + 0.119Z	22 ± 9
19	75°25.93′	13°59.30′	860	6	5.1	104 ± 3	1.109 + 0.066Z	140 ± 3
20	75°25.95′	14°21.80′	455	5	6.0	NL42–54	1.165 + 0.119Z	···
21	75°27.47′	14°40.17′	390	4	6.7	NL64–67	0.096 + 0.133Z	···
22	75°25.61′	13°48.56′	1014	6	7.7	56 ± 7	1.040 + 0.119Z	84 ± 8
23	75°23.96′	13°38.93′	1165	4	3.9	61 ± 2	1.040 + 0.119Z	81 ± 4
24	75°23.07′	13°23.84′	1344	4	3.9	63 ± 2	1.040 + 0.119Z	84 ± 1
25	75°22.11′	13°10.37′	1511	4	3.9	75 ± 3	0.798 + 0.138Z	86 ± 2
26	75°21.01′	12°53.57′	1700	4	3.9	72 ± 4	0.798 + 0.138Z	82 ± 4
27	75°19.88′	12°37.80′	1858	4	3.9	72 ± 2	0.798 + 0.138Z	82 ± 3
28	75°16.36′	11°59.50′	2169	4	3.9	59 ± 1	0.923 + 0.062Z	64 ± 2
29	75°13.43′	11°21.18′	2358	6	4.2	89 ± 5	0.923 + 0.062Z	96 ± 4
30	75°10.06′	10°43.27′	2460	3	3.6	86 ± 4	0.923 + 0.062Z	94 ± 5
31	75°06.76′	10°08.76′	2506	4	5.2	111 ± 5	0.923 + 0.062Z	126 ± 7
32	75°03.40′	09°32.64′	2595	7	8.1	149 ± 3	0.923 + 0.062Z	176 ± 6
34A	74°57.51′	08°43.16′	2642	4	3.9	247 ± 5	0.923 + 0.062Z	264 ± 11
34B	74°57.44′	08°42.97′	2642	4	3.9	242 ± 6	0.923 + 0.062Z	258 ± 10
35A	74°56.23′	08°22.91′	3347	4	3.9	>130	0.923 + 0.062Z	>161
35B	74°56.23′	08°22.91′	3347	4	3.9	>125	0.923 + 0.062Z	>160
36	75°18.90′	12°18.30′	2026	7	8.6	54 ± 1	0.923 + 0.062Z	65 ± 2
37	75°26.06′	13°55.21′	880	6	6.7	NL	1.109 + 0.066Z	···
38	75°22.90′	13°14.37′	1448	4	6.7	69 ± 2	0.798 ± 0.066Z	94 ± 4
39	75°21.73′	13°01.86′	1586	6	5.7	67 ± 2	0.765 ± 0.153Z	92 ± 2

NL, nonlinear gradient. From *Crane et al.* [1989]. Z indicates depth down to core.

A glance at Figure 4 reveals the distribution of heat flow data points from which the contours of observed heat flow are drawn. It is readily apparent that there are three swaths of high heat flow. One such region lies along the axis of the Knipovich Ridge and swings to the NW across the Molloy Ridge and into the Lena Trough. Another region is oriented subparallel to the Lena Trough but is located on the top of the shallow Yermak Plateau. This thermal anomaly is aligned along a structural extension of the Woodfjord on Svalbard known for its Quaternary volcanic activity. The third thermal anomaly lies along the Hornsund fault zone adjacent to Svalbard.

Using the Hutchison model [*Hutchison*, 1985; *Crane et al.*, 1988], we calculate what the surface heat flow should be (predicted HF) for each station, given a half spreading rate and a sedimentation rate that is calculated by knowing the decompacted sediment thickness and the modeled age of the crust below (Tables 5–7). In this manner, by comparing the predicted surface heat flow with the observed, we can estimate the half spreading rate across the Knipovich Ridge. We must go through these steps to find the spreading rate because there are no discernable magnetic anomalies in the region. If these models are appropriate, then one can estimate the age of the continental/oceanic crustal transition. Once these comparisons have been made, we can investigate the asymmetric extension models more thoroughly.

Shear Zones as Transtensional Margins Thermal and Structural Models of Opening

There is an infinite variety of strain patterns which produce asymmetric rift development. Here we will consider three classes of strain patterns which are not symmetric. We calculate the thermal and isostatic effect of a given strain field on the evolving rifted crust.

Asymmetric Pure Shear Extension

Asymmetric pure shear causes extension of the lithosphere composed of a brittlely deforming upper layer over a ductily deforming lower layer producing an asymmetric lithospheric cross section as a result of migration of the rift walls in a direction not coinciding with the direction of spreading. The model may be characterized as migrating symmetric pure shear. We first define a region of pure shear

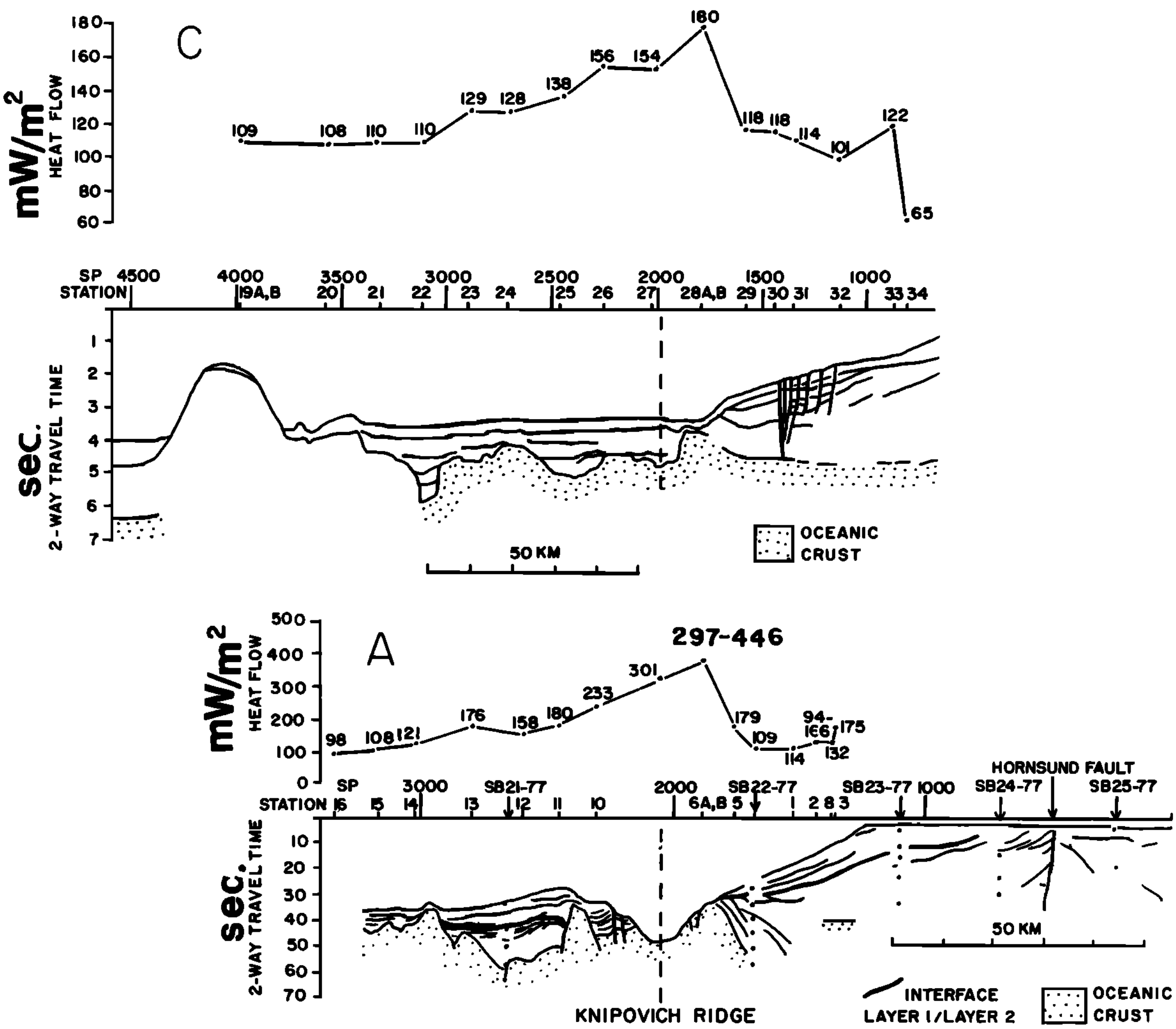

Fig. 6. Seismic cross sections of lines A and C (Figure 5), with observed heat flow superimposed. Depths to subsurface are estimated in seconds of two-way travel time.

extensional deformation, with fixed width W_0, as was done by *Buck et al.* [1988]. The lithospheric plates on either side of this extension zone are taken to move in opposite directions with a velocity difference of $2u_r$. The horizontal gradient of horizontal velocity ($\partial u/\partial x$) is constant across the width of the extending region and is equal to the vertical gradient of vertical velocity ($\partial w/\partial z$).

In a frame of reference in which one plate (plate 1 on the left side of Figure 3*a*) is fixed, the boundaries of the shearing region have velocities u_{b1} and u_{b2}. If $u_{b1} = u_{b2} = u_r$, then symmetric extension results. We will consider models with other velocities for the rift boundaries, which can lead to narrowing of the region of extension and/or to asymmetric extension. A simple example of asymmetric extension is for $u_{b1} = u_{b2} = 2u_r$. This produces no narrowing of the rift zone but results in the center of that zone remaining a fixed distance from the right-hand margin as it moves away from the left margin.

Simple Shear Extension

Simple shear along a throughgoing low-angle detachment [after *Wernicke*, 1985] divides the lithosphere into an "upper plate" and a "lower plate" or hanging wall and footwall. Thinning of the lower lithosphere is offset along the detachment from thinning of the upper lithosphere, producing an asymmetric lithospheric cross section. Large topographic offsets are produced (i.e., tens of kilometers, for very large horizontal offsets), and therefore there must be some additional distributed strain, referred to as isostatic response strain (Figure 3*b*). We use the model approach of *Buck et al.* [1988]. For the simple shear model the important parameters are the width of the shear zone, W_{ss}, and the dip of the shear zone or detachment, θ.

Thermal Calculation

After the velocity fields are defined, the two-dimensional equation of advective and diffusive heat transport is solved:

$$\partial T/\partial t + u\partial T/\partial x + w\partial T/\partial z = k(\partial T^2/\partial x^2 + \partial T^2/\partial z^2)$$

where

T	temperature, °C;
t	time;
k	diffusivity;
x, z	horizontal and vertical directions;
u, w	horizontal and vertical velocities.

TABLE 5. Molloy Ridge Heat Flow Versus Age

Station	Decompacted Thickness, m	Half Spreading Rate, mm yr^{-1}: 6.0 Age	6.0 SR	6.0 HF	4.0 Age	4.0 SR	4.0 HF	3.4 Age	3.4 HF	3.0 Age	3.0 SR	3.0 HF	Observed HF
						East							
Y13	2,400	2.8	857	284	4.2	571	233			5.6	429	203	178
83	2,400	4.6	522	228	6.9	349	188			9.2	261	159	115
Y14	2,900	7.0	414	183	10.5	276	154			14.0	207	131	120
84	2,900	8.0	363	171	12.0	242	143			16.0	182	123	115
40	10,100	10.8	935	157	16.2	623	132			21.6	468	115	93
85	5,925	11.2	529	150	16.8	353	125			22.4	265	110	99
39	8,350	12.2	684	150	18.3	456	124			24.4	342	109	87
88	8,350	12.4	673	149	18.6	449	122			24.8	337	108	108
38	7,210	13.8	522	138	20.7	348	116			27.6	261	102	117
86	7,400	14.4	514	136	21.6	343	112			28.8	257	99	103
37	7,210	15.6	462	131	23.4	308	108			31.2	231	95	116
31	5,350	16.2	330	127	24.3	220	106			32.4	165	92	114
36	7,210	17.4	414	125	26.1	276	104			34.8	207	91	107
32	8,160	17.8	458	125	26.7	306	104			35.6	229	91	101
35	7,210	19.0	379	121	27.5	262	102			38.0	190	88	85
33	10,100	19.4	520	122	28.1	359	103			38.8	260	90	122
34	10,100	20.0	505	121	30.0	337	100			40.0	253	88	65
						West							
50	0	1.2	···	450	1.8	···	365	2.1	342	2.4	···	318	285
51	0	2.8	···	297	4.2	···	242	4.9	224	5.6	···	210	200
80	0	3.6	···	264	5.4	···	216	6.3	203	7.2	···	187	274
82	0	4.0	···	246	6.0	···	204	7.0	187	8.0	···	180	144
79	0	8.2	···	178	12.3	···	145	14.1	135	16.4	···	126	166
78	0	8.4	···	176	12.6	···	144	14.7	133	16.8	···	124	161
77	0	9.4	···	166	14.1	···	135	16.5	125	18.8	···	118	123
Y12	0	17.6	···	122	26.4	···	98	30.8	92	35.2	···	86	111

Age, age of the crust, Ma; SR, sedimentation rate, m/m.y.; HF, heat flow predicted by the model for a certain spreading rate and sedimentation rate, mW m^{-2}, and observed HF, observed ehat flow, mW m^{-2}.

The conductivity of the crust and the mantle can be varied, and the boundary temperatures are $T = 0°C$ on the top boundary ($z = 0$ km) and $T = 1300°C$ on the bottom boundary ($z = 125$ km). Material passes through the sides if the velocity is nonzero at that point. Crustal thickness is calculated from the position of the advected Moho.

A finite difference method is used to solve the temperature equation and an equation for advection of the base of the crust (the Moho) at points on a fixed Eulerian grid representing the lithosphere. Heat flow is the product of the vertical derivative of temperature and conductivity. Subsidence and uplift are calculated under the assumption of local isostatic compensation with a given density contrast between the crust and the mantle and a given thermal expansion coefficient (α). The elevation of a point on the surface depends on the average density of a column of material beneath that point. For all the calculations here we take $\alpha = 3.0 \times 10^{-5}$, the crustal thickness is 32 km, the mantle density is 3300 kg m^{-3}, the crustal density is 2800 kg m^{-3}, and the initial lithospheric thickness is 125 km.

TABLE 6. East Knipovich Flank, Heat Flow Versus Age

Station	Decompacted Thickness, m	Observed HF	Half Spreading Rate, mm yr^{-1}: 6.0 Age	6.0 SR	6.0 HF	4.0 Age	4.0 SR	4.0 HF	3.0 Age	3.0 SR	3.0 HF
6–83	3,000	371	2.0	1500	335	3.0	1000	279	4.0	750	246
6	3,560	250	2.6	1369	306	3.9	913	246	5.2	685	218
5–83	3,250	179	3.6	903	256	4.4	739	236	7.2	452	183
5	4,610	138	4.0	1152	244	6.0	768	203	8.0	576	173
4–83	8,400	109	4.6	1827	242	6.9	1217	199	9.2	914	167
4	7,610	112	5.9	1290	213	8.9	855	174	11.8	645	152
1–83	7,290	114	6.6	1105	198	9.9	736	165	13.2	533	141
3	11,080	100	7.6	1458	194	11.4	972	159	15.2	729	139
8–83	6,730	132	8.4	801	178	12.6	534	146	16.8	401	128
3–83	6,730	130	8.6	783	176	12.9	522	145	17.2	392	126

Age, age of the crust, Ma; SR, sedimentation rate, m/my; HF, (predicted heat flow for various spreading and sedimentaiton rates, mW m^{-2}; observed HF, observed heat flow, mW/m^{-2}.

TABLE 7. West Knipovich Flank, Heat Flow Versus Age

			20 Ma HSR = 7.9			30 Ma HSR = 5.3			40 Ma HSR = 4.0		
Station	Decompacted Thickness, m	Observed HF	Age	SR	HF	Age	SR	HF	Age	SR	HF
96	320	301	0.8	400	528	1.2	267	441	1.6	200	377
94	2413	197	1.2	2010	437	1.8	1341	355	2.4	1005	308
92	1500	125	2.2	682	325	3.3	455	268	4.4	341	233
7	105	135	2.6	40	312	3.9	27	255	5.2	20	222
28	320	180	2.8	114	296	4.2	76	243	5.6	352	211
10–83	1970	233	2.8	704	290	4.2	469	236	5.6	352	208
11–83	5280	180	4.2	1257	243	6.3	838	197	8.4	629	175
8	2110	159	4.4	480	234	6.6	320	190	8.8	240	168
91	2735	139	4.4	622	235	6.6	414	190	8.8	311	168
27	1950	154	4.8	406	221	7.2	271	182	9.6	203	161
89	1944	113	5.0	389	220	7.5	259	181	10.0	194	157
12–83	5850	158	5.4	1083	216	8.1	722	180	10.8	542	156
9	1360	125	5.8	235	204	8.7	156	168	11.6	117	146
90	1644	137	6.6	249	190	9.9	166	158	13.2	125	137
10	810	179	6.8	119	190	10.2	79	156	13.6	60	136
26	2570	156	7.0	367	187	10.5	245	154	14.0	184	134
13–83	1660	176	7.0	237	187	10.5	158	154	14.0	119	134
42	4270	122	7.8	548	181	11.7	365	149	15.6	274	130
11	1500	81	8.2	183	173	12.3	122	142	16.4	91	124
14–83	520	121	9.2	57	165	13.8	38	135	18.4	29	118
25	2900	138	9.4	309	163	14.1	206	134	18.8	154	117
12	810	108	9.4	86	163	14.1	57	134	18.8	43	116
43	3233	125	10.2	317	158	15.3	211	130	20.4	159	113
15–83	1230	108	10.4	118	154	15.6	79	127	20.8	59	111
13	105	116	11.0	9	153	16.5	6	125	22.0	4	107
24	1080	128	11.8	92	145	17.7	61	120	23.6	46	104
14	1350	103	12.2	111	143	18.3	74	117	24.4	56	102
15	0	149?	13.2	0	138	19.8	0	115	26.4	0	99
23	1640	129	13.4	122	137	20.1	82	113	26.8	61	98
16	810	89	14.6	55	131	21.9	37	108	29.2	28	93
53	3240	107	15.0	216	131	22.5	144	108	30.0	108	94
22	2740	110	15.2	180	130	22.8	120	107	30.4	90	93
17	810	119	15.8	51	126	23.7	34	104	31.6	26	90
45	2900	97	16.2	179	124	24.3	119	104	32.4	90	90
18	105	70	16.8	6	122	25.2	4	102	33.6	3	88
21	1210	110	17.2	70	121	25.8	47	100	34.4	35	87
52	320	133	18.4	17	118	27.6	12	97	36.8	9	84
20	440	108	19.0	23	116	28.5	15	95	38.0	12	83
46	2740	102	20.0	137	114	30.0	91	94	40.0	69	82

Station, in order of distance from the Knipovich Ridge; HSR, half spreading rate, mm/yr; SR, sedimentation rate, m/m.y.; HF, predicted heat flow for various spreading and sedimentation rates, mW m^{-2}; Age, age of the crust, Ma; Observed HF, observed heat flow, mW m^{-2}.

Ridge Jump Extension

Ridge jump extension (Figure 3*c*) is modeled using a lithosphere composed of a brittlely deforming upper layer over a ductally deforming lower layer producing an asymmetric lithospheric cross section resulting from the jumping of the rift axis. It is similar to the asymmetric pure shear model but allows for a jump in the center of extension at a set time. The way this is implemented is for symmetric extension ($u_{b1} = u_{b2} = u_r$) to be imposed until time t^2, and then the positions of the boundaries are moved, while the velocities remain the same. The final results create an overall pattern of asymmetric heat flow and topography (but symmetric at each ridge), although the interior steps may be formulated from two or more separate episodes of pure shear extension. The asymmetric pure shear extension model can be thought of as being produced by an infinite number of infinitesimal offset ridge jumps.

RESULTS

If we group the heat flow data into the following regions: (1) the east flank of the Molloy Ridge (Table 5), (2) the west flank of the Molloy Ridge (Table 5), (3) the east flank of the Knipovich Ridge (Table 6), and (4) the west flank of the Knipovich Ridge (Table 7), and plot the predicted heat flow calculated for specific spreading rates versus the observed data, then we can determine the best fits to the *McKenzie* [1978] cooling plate model (Figures 7–9). For the Molloy Ridge the best fit to a cooling plate model yields a half spreading rate of 3.4 mm yr^{-1} on the western flank and 3.0 mm yr^{-1} on the eastern flank yielding a full spreading rate of 6.4 mm yr^{-1} (Figure 10). By comparison, *Thiede et al.* [1990] suggest a similar spreading rate on the eastern flank based on the distance between chron 5 and the recent neovolcanic zone. These estimates of spreading rate differ significantly from the 16 mm yr^{-1} estimate presented by *Vogt et al.* [1981]

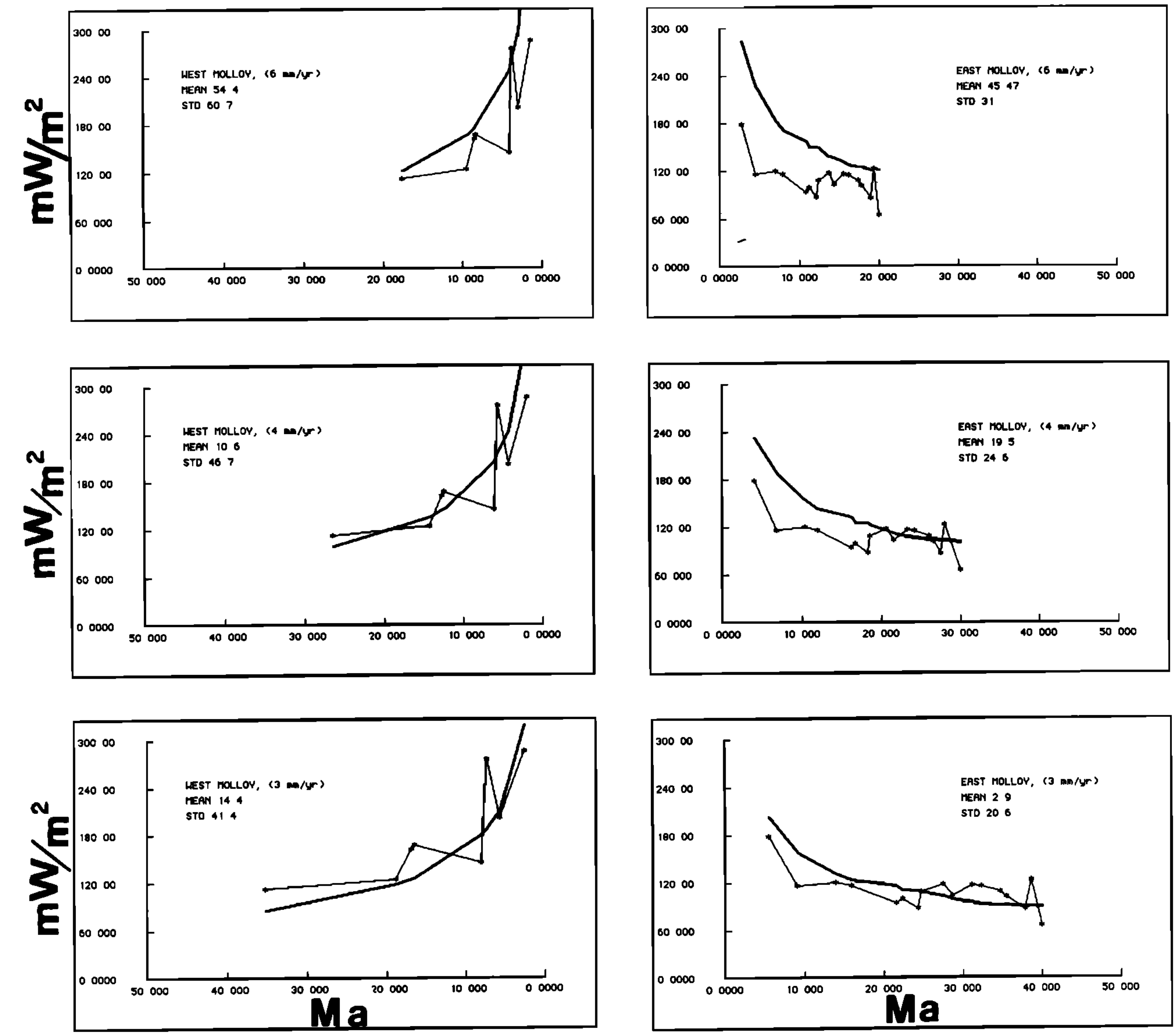

Fig. 7. Predicted heat flow (in milliwatts per square meter) versus age (in mega annum) across the Molloy Ridge compared to predicted heat flow determined from the *McKenzie* [1978] cooling plate model (bold curve). The three different cases represent half spreading rates of 3, 4, and 6 mm yr^{-1}. Details of the stations are found in Table 5.

and *Eldholm et al.* [1990]. If our heat flow determined spreading rates are correct, then the initiation of seafloor spreading near the Molloy Ridge (from 78°30'N to 79°30'N) might have begun at 40–50 Ma (taking the Hornsund fault zone as the position for oceanic/continental crustal transition).

Across the Knipovich Ridge the best fit between the observed heat flow data and the cooling plate model suggests a half spreading rate of 4.0 mm yr^{-1} on the western flank and 3.0 mm yr^{-1} on the eastern flank, yielding a full spreading rate of 7.0 mm yr^{-1}. These results suggest a continent/ocean transition age of 20–30 Ma at a latitude of 78°N–78°30'N. However, the goodness of fit between the observed and predicted heat flow on the eastern flank is very poor.

At the southern latitude of 75°N the best fit of the heat flow data to the cooling plate model yields a continent/ocean transition age of 60 Ma (with a half spreading rate of 4.5 mm yr^{-1}). Complicating the relatively good fit is a band of high heat flow associated with the eastern Hornsund fault escarpment adjacent to this section of the continental margin (Figure 4).

In general, asymmetric heat flow prevails across the northern Knipovich Ridge, and in all cases there is a very poor fit between data from the eastern flank and the cooling plate (pure shear) model. The data across the Molloy Ridge on the other hand yield a much better fit with the pure shear model (Figure 10).

It is this mismatch between the goodness of fit on the eastern and the western flanks of the Knipovich Ridge with the pure shear models that has persuaded us to test the asymmetric pure shear, the simple shear detachment fault, and the ridge jump models against the available heat flow and topographic data.

When the asymmetric pure shear models are compared to

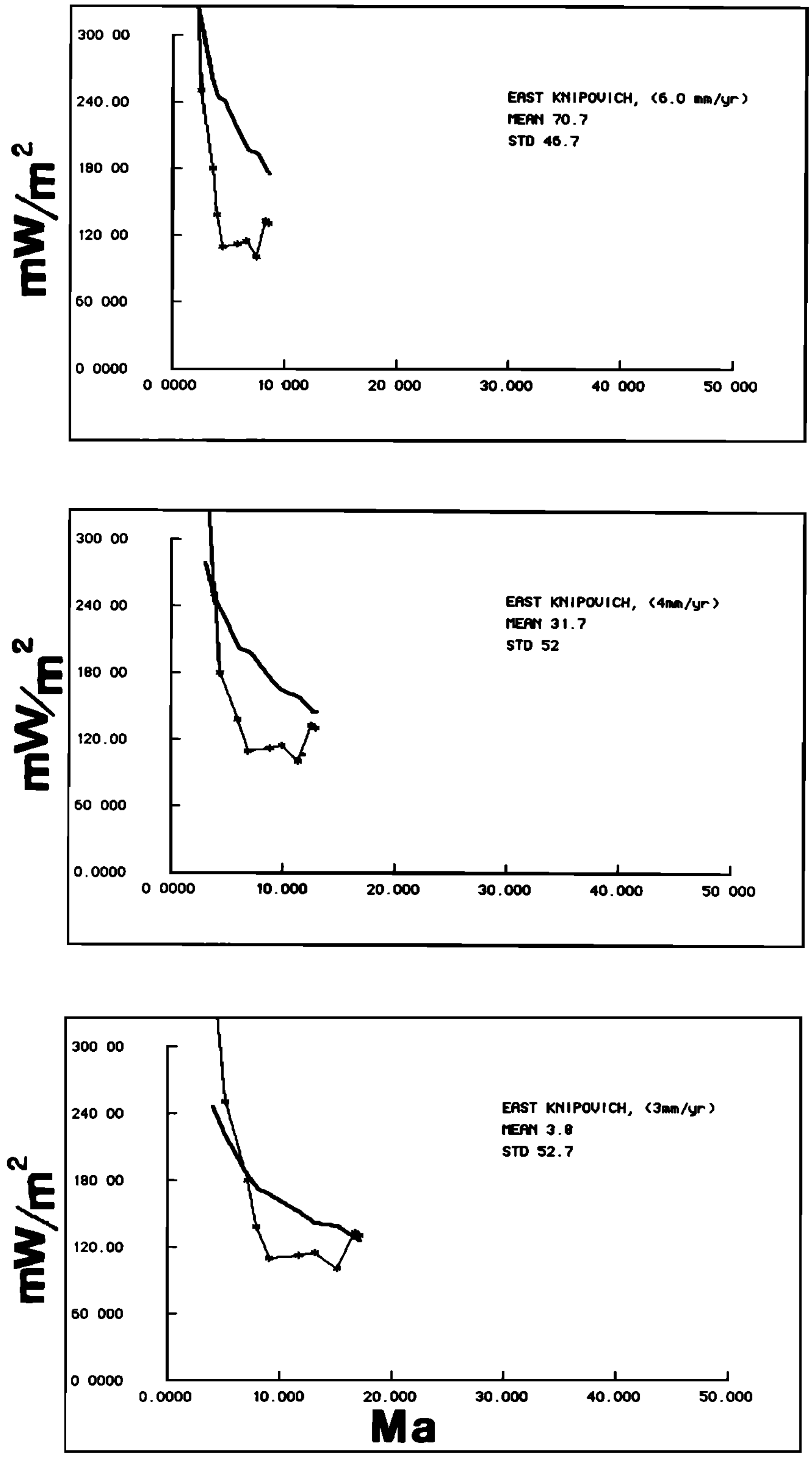

Fig. 8. Predicted heat flow (in milliwatts per square meter) versus age (in mega annum) across the eastern flank of the Knipovich Ridge compared to predicted heat flow determined from the cooling plate model (bold curve). The three different cases represent half spreading rates of 3, 4, and 6 mm yr^{-1}. Note the poor fit between the predicted heat flow and the cooling plate model. Details of the stations are found in Table 6.

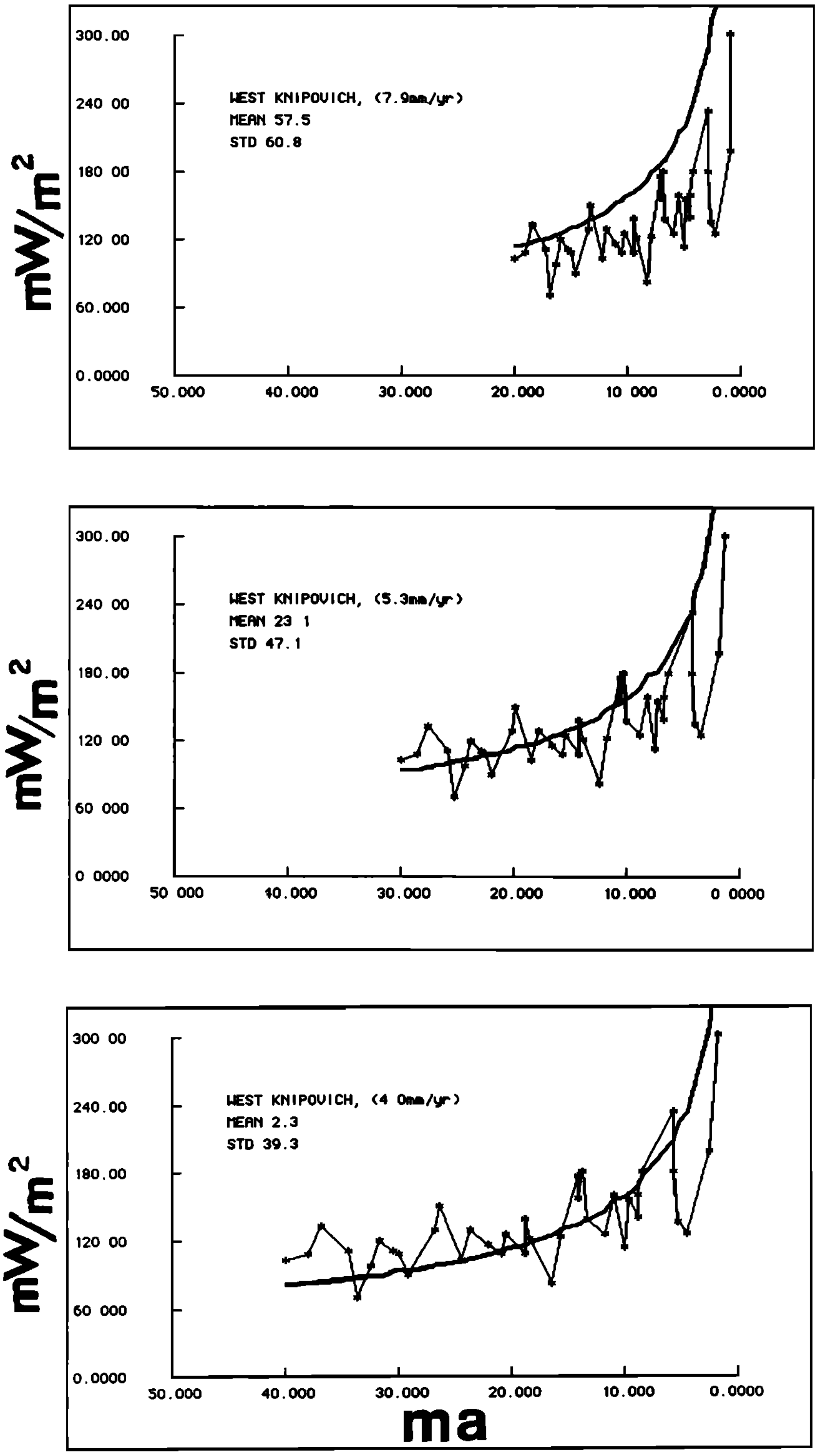

Fig. 9. Predicted heat flow (in milliwatts per square meter) versus age (in mega annum) across the western flank of the Knipovich Ridge compared to predicted heat flow determined from the cooling plate model. The three different cases represent half spreading rates of 4, 5.3 and 7.9 mm yr^{-1}. Details of the stations are found in Table 7.

the data, there is an excellent fit between the observed and predicted heat flow and topography for the case where the western flank is spreading at 7 mm yr^{-1} and the eastern flank at 1 mm yr^{-1} (Figure 11). This asymmetry keeps the axis pinned on the eastern margin of the basin. In order to generate very high heat flow at the axis the initial rift width is very narrow, and in this case we have chosen a width of 19 km and allowed the rift to evolve for 45 m.y.

Figures 12 and 13 depict the comparisons of measured to calculated heat flow and topography for spreading occurring

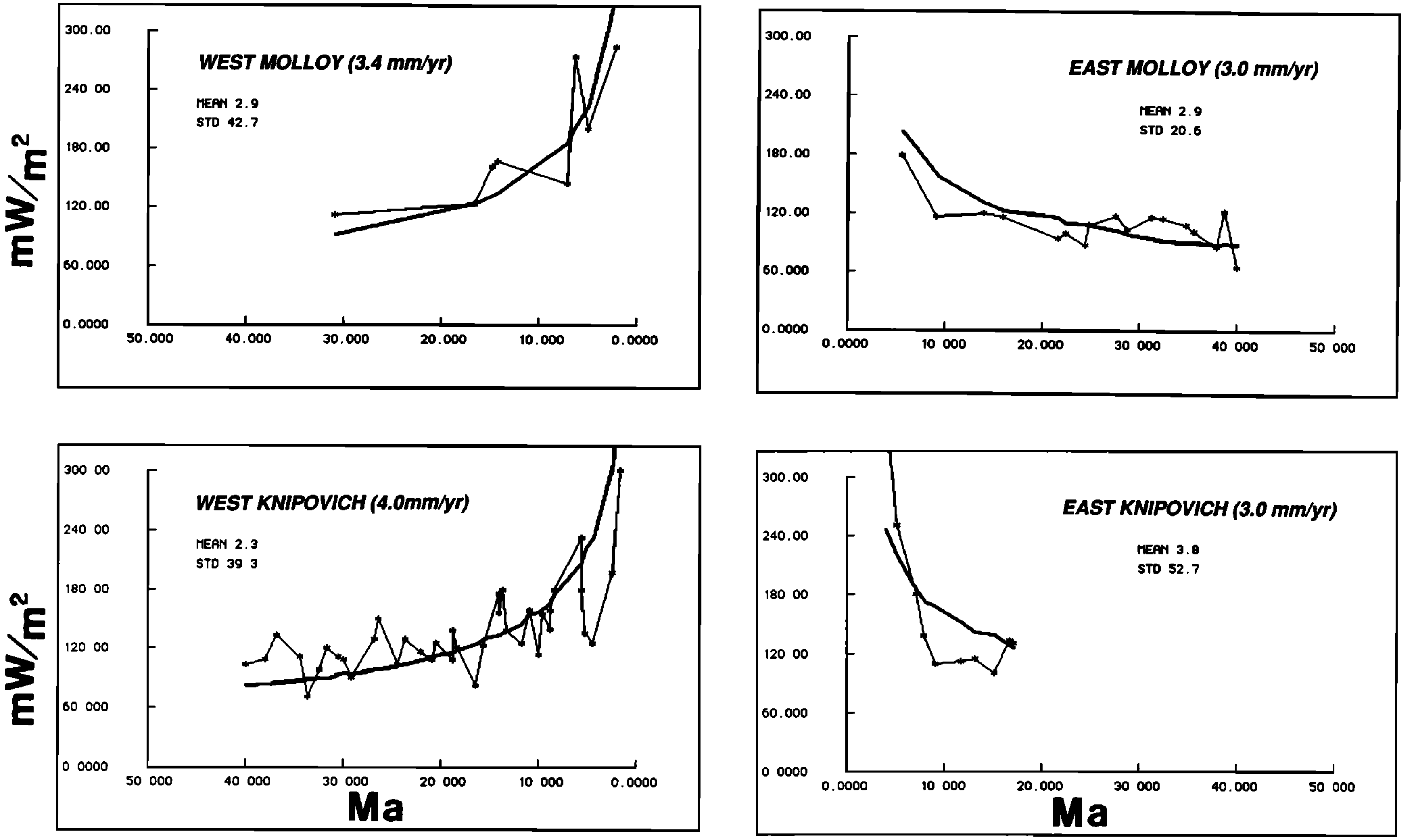

Fig. 10. The best fits between the predicted heat flow (in milliwatts per square meter) versus age (in mega annum) and the cooling plate model for the Molloy Ridge and the Knipovich Ridge. The results yield a full spreading rate of 6.4 mm yr^{-1} across the Molloy Ridge and 7 mm yr^{-1} across the Knipovich Ridge. Note the poor fit on the eastern side of Knipovich Ridge.

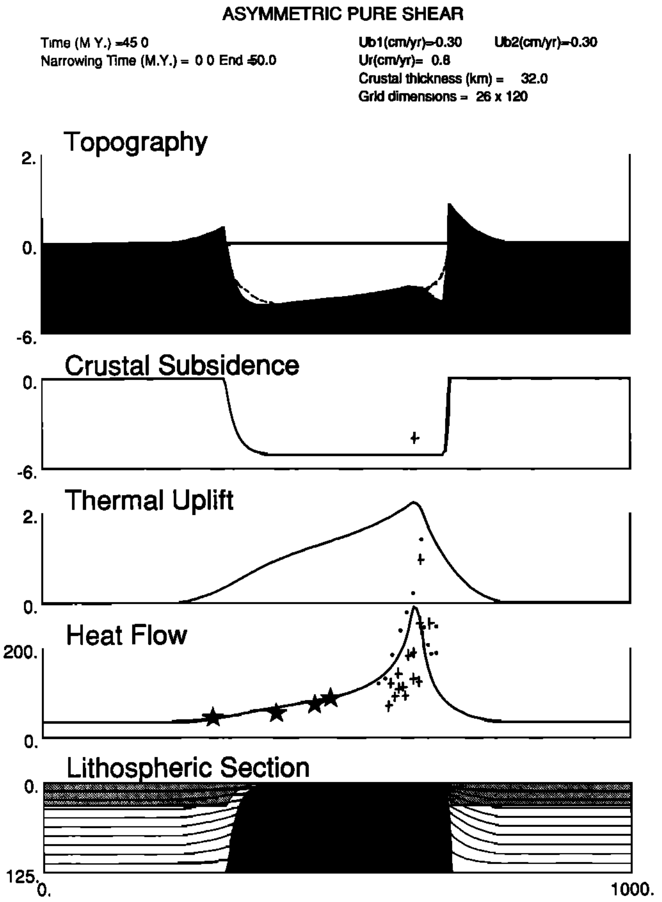

Fig. 11. The best fit between all of the heat flow data collected across the Knipovich Ridge (corrected for the cooling effects of sedimentation using the Hutchison model) with the asymmetric pure shear model evolved to 45 Ma at a spreading rate of 8 mm yr^{-1}. The initial rift width was 19.2 km; the initial crustal thickness was 32 km (lightly shaded region); and the velocity that the ridge migrates to the east is 3 mm yr^{-1}, yielding a net spreading rate of 7 mm yr^{-1} to the west and 1 mm yr^{-1} to the east. The heat flow stations are indicated by dots (Flunorge 1983), crosses (Svalbard 1984), and stars (Vema). The observed depth to basement, corrected for sediment loading, is dotted across the solid, predicted-topography profile (which is the sum of the calculated crustal subsidence and the thermal uplift). Horizontal and vertical scales (in kilometers). Resultant heat flow (in milliwatts per square meter). Curvilinear lines in the lithospheric section represent isotherms, the darkly shaded region indicates upwelled asthenosphere. Solid region under the rise axis indicates magma. Grid dimensions, 26 × 120 cells.

along low (15°) to high-angle (45°) detachment faults. In these examples we chose the rift axis of the Knipovich Ridge to be the point where the detachment fault hits the seafloor. The fault was assumed to dip towards Svalbard, making this nearby island a part of the upper plate. In the analysis we attempted models with full spreading rates ranging from 4 to 10 mm yr^{-1} and an initial crustal thickness ranging from 10 to 32 km. From the two examples depicted, the case where the detachment angle is low (15°) does not fit the observed heat flow data. However, the width of the predicted ocean basin is approximately the same as the observed width yet the predicted depth to basement is much shallower than in reality and the calculated heat flow is far too low to be a viable model.

The case for a detachment fault angle of 45° and a full spreading data of 8 mm yr^{-1} yields a much better fit with both the heat flow and topographic data when the model is allowed to evolve for 40 m.y. However, a true simple shear model should only accommodate low-angle detachments. A fault as steep as 45° generates a pattern of strain in the crust which is essentially considered a case of asymmetric pure shear.

In the case of a rift jumping eastward from one position to another in the Norwegian-Greenland Sea (Figures 14*a* and 14*b*) we observe a good fit with a model that undergoes 25 m.y. of pure shear extension and then jumps 150 km to the east and spreads for an additional 20 m.y. at a full spreading rate of 8 mm yr^{-1}. However, in this case the predicted topography is from 1 to 2.5 km shallower than is observed.

In summary, observations suggest that the shallow angle detachment fault model is not viable. On the other hand, the asymmetric pure shear and the high-angle detachment models have the best fit with both heat flow and topographic data. These models suggest that spreading initiated between 40 and 45 Ma at a latitude of 78°N, in contrast to the 20–30 Ma estimate derived from the comparison of the data with the cooling plate model.

IMPLICATIONS

Crane et al. [1982] suggested that the Molloy Ridge could have initially formed as a pull-apart basin within the Spitsbergen Shear Zone. They suggested that either (1) the Nansen Ridge propagated from the Arctic Ocean in the north into the Spitsbergen Shear Zone, generating extensional deviatoric stress across this region, allowing for the intrusion of mantle material in the Molloy Ridge area, or (2) the Knipovich Ridge propagated from the south generating the same feature. If the cooling plate models are correct, then the Molloy Ridge formed 20–30 m.y. before the Knipovich Ridge ever reached a latitude of 78°N. Thus the Molloy Ridge may have been created as a pull-apart basin or "extensional relay zone" in response to a readjusting and propagating Nansen Ridge plate boundary.

On the basis of structural and heat flow data, *Crane et al.* [1988] suggested that the Knipovich Ridge propagated north of 78°N at about 14 Ma, deactivating a former "transform" now known as the Hovgård Ridge located in the Boreas Basin. Additional evidence for regional thermal rejuvenation between 16 and 10 Ma was cited by *Feden et al.* [1979], who suggested that the Nansen Ridge underwent an episode of increased volcanic activity beginning at chron 5b. This activity must have been regional in scope as volcanism developed on northern Svalbard around 12 Ma continuing into the Quaternary. Whether the volcanic episode on Svalbard is attributed to the northward propagation of the Knipovich Ridge or the thermal rejuvenation and southward propagation of the Nansen Ridge is not known.

If the asymmetric pure shear or detachment models are correct, then the northernmost Knipovich Ridge formed only 5–10 m.y. after the Molloy Ridge. It is clear that the preexisting faults on the Yermak Plateau and on neighboring Svalbard may be future loci for volcanic eruptions, depending on the direction and magnitude of propagation events

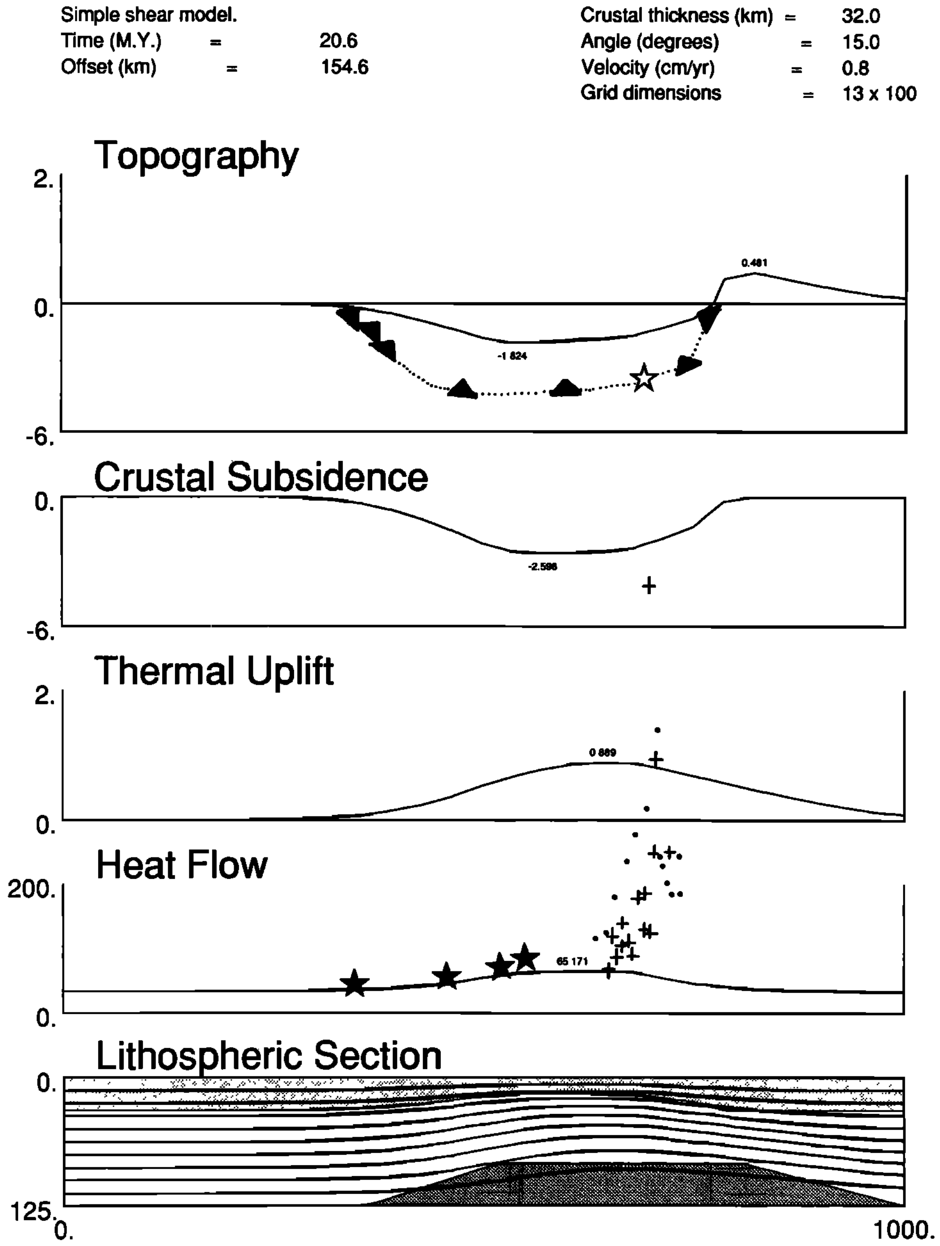

Fig. 12. The best fit between a simple shear model (depicting 20 m.y. of evolution at a spreading rate of 8 mm yr^{-1} along a detachment fault dipping 15° to the east underneath Svalbard) and corrected topography and heat flow data. Heat flow stations are as indicated in Figure 11, and are superimposed on the heat flow curve. Topography corrected for sediment loading is shown by triangles and is superimposed on the predicted bathymetry profile. The open star indicates the Knipovich Ridge axis. The initial crustal thickness was 32 km and the offset across the ridge axis at 20 Ma is 154.6 km. Grid dimensions, 13 × 100 cells.

from both the Nansen and Knipovich ridges. More heat flow data collected north of Svalbard should reveal the extent of the thermal rejuvenation of this continental margin caught between two dueling spreading centers.

Conclusions

The analysis of heat flow and topographic data collected in the northern Norwegian-Greenland Sea reveals an asymmetric evolution of the Eurasian and North American plates about the Knipovich Ridge. A test of the asymmetric pure shear, asymmetric simple shear, and ridge jumping models against these data suggest that most likely, rifting is or has been occurring in the asymmetric pure shear or high-angle simple shear mode centered on a system of faults adjacent to the continental margin of Svalbard. One must also consider the case for an eastward jumping ridge as is suggested not only by the good fit to the data but also by the occurrence of

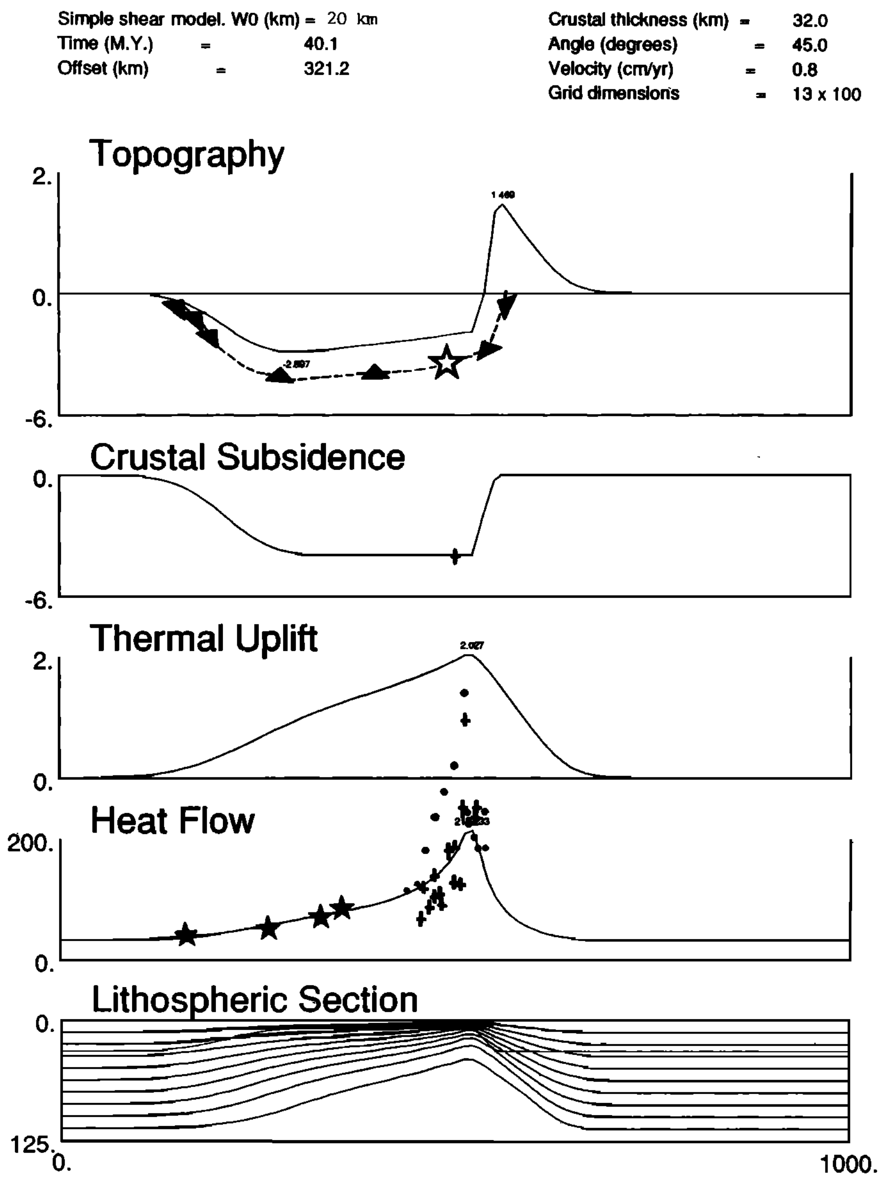

Fig. 13. The best fit between all of the heat flow data collected across the Knipovich Ridge and a simple shear model with a detachment fault dipping 45° to the east (underneath Svalbard). Heat flow stations are as indicated in Figure 11, corrected for the cooling effects of sedimentation using the Hutchison model. This fit suggests the oceanic crust has been evolving for 40 Ma at a spreading rate of 8 mm yr^{-1} at a latitude of 78°N. In this case the initial axial width was 20 km; the crustal thickness was 32 km at the initial point of rifting, and the present-day offset is 321 km. Grid dimensions, 13 × 100 cells.

high heat flow located on the Svalbard margin and atop the Yermak Plateau.

These two bands of high heat flow located more than 70–150 km off the axis of the Knipovich Ridge conflict with the theory that intrusion, extension, and rifting are initiated along only one fault. Instead, the data suggest that when rifting occurs along and within a formerly active continental shear zone, the region of extension may not be limited to only one narrow fault but could occur first over several faults many tens of kilometers apart or could relocate from one fault to another, creating a net asymmetric pattern of heat flow and topography in the process.

We suggest that the present Knipovich Ridge plate boundary was borrowed from preexisting fault(s) within the ancient Spitsbergen Shear Zone. That one or several faults may still be actively inclined beneath Svalbard is suggested by the high concentration of seismic activity within the Eurasian plate adjacent to and on Svalbard contrasting to the low level of seismicity on the opposing North American plate.

To verify that the Knipovich Ridge has always been located within the ancient Spitsbergen Shear Zone and that this ancient shear is the major fault system along which present-day rifting is taking place, one needs to collect more heat flow and structural data between the Knipovich Ridge

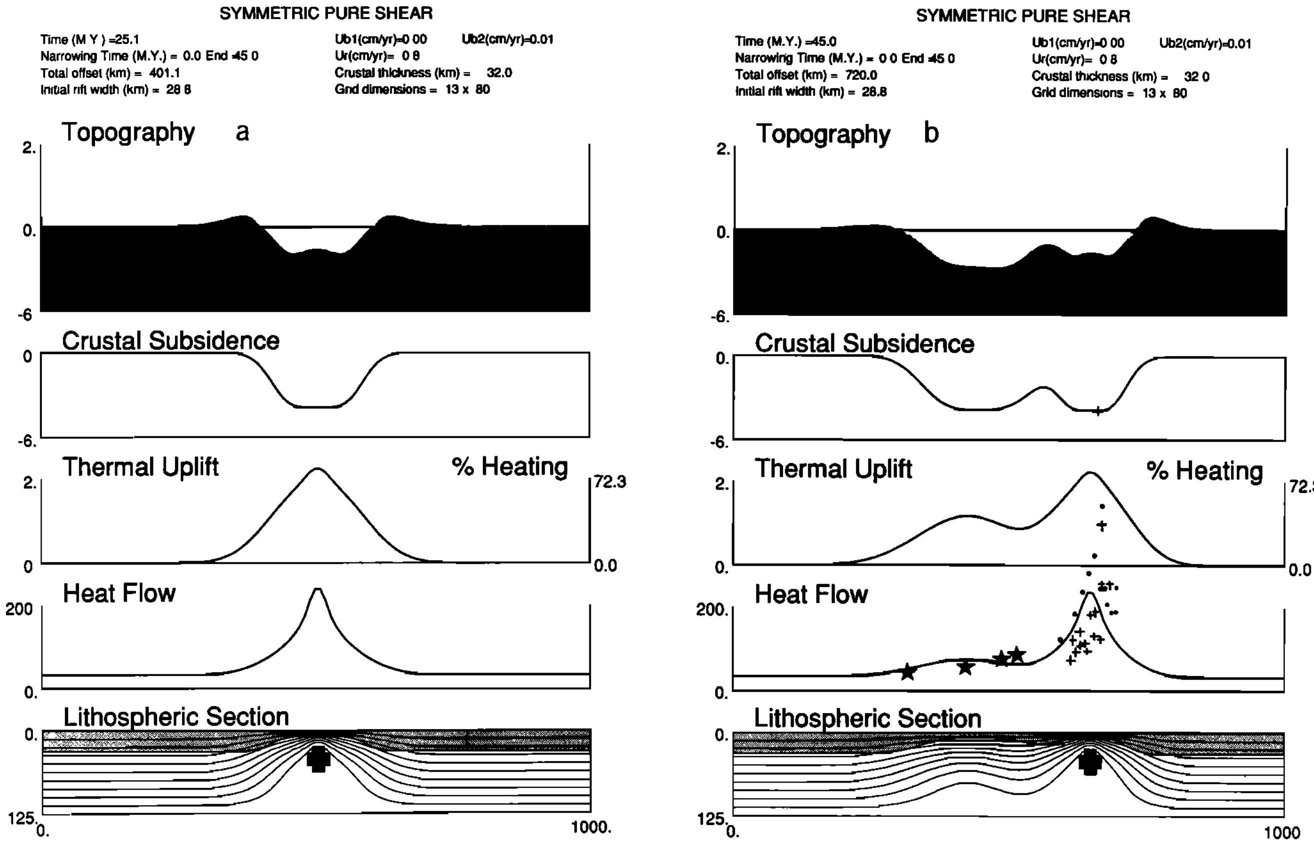

Fig. 14. The best fit between all of the heat flow data and a ridge jump model. Heat flow data are from Flunorge 1983 (dots), Svalbard 1984 (crosses), and Vema (stars), (corrected for the cooling effects of sedimentation using the Hutchison model). (*a*) The ridge jump model at 25 Ma. (*b*) The ridge jump model evolved to 45 Ma after a 150 km eastward jumping of the axis at 25 Ma. In this model the full spreading rate is 8 mm yr^{-1}. Grid dimensions, 13 × 80 cells.

and the continental margin of Greenland to verify that the rise axis has not simply been jumping to the east throughout 60 m.y. of its history.

Acknowledgments. The authors would like to thank the Seismological Observatory of the University of Bergen for providing 2 months of ship time on the R/V *Haakon Mosby*. Data collection and processing were funded by the Norwegian Petroleum Directorate, Elf Aquitaine, Norge, and the U.S. Office of Naval Research (grant N00014-90-1106). This manuscript benefited substantially from Peter Vogt's thoughtful reviews.

REFERENCES

Birkenmajer, K., The geology of Svalbard, the western part of the Barents Sea and the continental margin of Scandinavia, in *The Ocean Basins and Margins*, vol. 5, *The Arctic Ocean*, edited by A. E. M. Nairn and M. Churkin, pp. 265–330, Plenum, New York, 1981.

Bonatti, E., and K. Crane, Oscillatory spreading explanation of anomalously old uplifted crust near oceanic transforms, *Nature*, *300*, 343–345, 1982.

Bonatti, E., and K. Crane, The geology of oceanic transform faults, *Sci. Am.*, *250*(5), 40–51, 1984.

Buck, W. R., F. Martinez, M. S. Steckler, and J. R. Cochran, Thermal consequences of lithospheric extension: Pure and simple, *Tectonics*, *7*(2), 213–234, 1988.

Chan, W. W., and B. J. Mitchell, Intraplate earthquakes in northern Svalbard, *Tectonophysics*, *114*, 181–191, 1985.

Courtillot, V., Propagating rifts and continental breakup, *Tectonics*, *1*, 239, 1982.

Crane, K., and E. Bonatti, Fracture zone control on the opening of the Red Sea: SIR A data, *J. Geol. Soc. London*, *144*, 407–420, 1987.

Crane K., O. Eldholm, A. M. Myhre, and E. Sundvor, Thermal implications for the evolution of the Spitsbergen transform fault, *Tectonophysics*, *89*, 1–32, 1982.

Crane K., E. Sundvor, J.-P. Foucher, M. Hobart, A. M. Myhre, and S. LeDouraran, Thermal evolution of the western Svalbard Margin, *Mar. Geophys. Res.*, *9*, 165–194, 1988.

Eldholm, O., A. M. Myhre, E. Sundvor, and J. I. Faleide, Cenozoic evolution of the margin off Norway and Svalbard, in *Petroleum Geology of the North European Margin*, edited by A. M. Spencer et al., pp. 3–18, Graham and Trotman, Detroit, Mich., 1984.

Eldholm, O., J. I. Faleide, and A. M. Myhre, Continent-ocean transition at the western Barents Sea/Svalbard continental margin, *Geology*, *15*, 1118–1122, 1987.

Eldholm, O., A. M. Karasik, and P. A. Reksnes, Geology of the Arctic Ocean region, in *The Geology of North America*, vol. L, *The North American Plate Boundary*, *DNAG Synthesis Volume*, edited by A. Grantz, G. L. Johnson, and J. Sweeney, pp. 171–184, Geological Society of America, Boulder, Colo., 1990.

Faleide, J. I., S. T. Gudlaugsson, and G. Jacquart, Evolution of the western Barents Sea, *Mar. Pet. Geol.*, *1*, 123–150, 1984.

Feden, R. H., P. R. Vogt, and H. S. Fleming, Mantle and bathymetric evidence for the Yermak hot spot of Svalbard in the Arctic Basin, *Earth Planet. Sci. Lett.*, *44*, 18–38, 1979.

Hutchison, I., The effects of sedimentation and compaction on oceanic heat flow, *Geophys. J. R. Astron. Soc.*, *82*, 439–459, 1985.

Johnson, G. L., J. R. Southall, P. W. Young, and P. R. Vogt, The origin and structure of the Iceland Plateau and Kolbeinsey Ridge, *J. Geophys. Res.*, *77*, 5688–5696, 1972.

Kovacs, L. C., and P. R. Vogt, Depth-to-magnetic source analysis of the Arctic Ocean region, *Tectonophysics*, *89*, 255–294, 1982.

LaBrecque, J. L., D. V. Kent, and S. C. Cande, Revised magnetic polarity time scale for late Cretaceous and Cenozoic time, *Geology*, *5*, 330–335, 1977.

Langseth, M. G., and G. W. Zielinski, Marine heat flow measurements in the Norwegian-Greenland Sea and in the vicinity of Iceland, in *Geodynamics of Iceland, the North Atlantic Area*, edited by L. Kristjansson, pp. 277–295, D. Reidel, Norwell, Mass., 1974.

Lister, G. S., M. A. Etheridge, and P. A. Symonds, Detachment faulting and the evolution of passive continental margins, *Geology*, *14*, 246–250, 1986.

McKenzie, D. P., Some remarks on the development of sedimentary basins, *Earth Planet. Sci. Lett.*, *40*, 25–32, 1978.

Minster, J. B., and T. H. Jordan, Present-day plate motions, *J. Geophys. Res.*, *83*, 5331–5354, 1978.

Morgan, W. J., Hotspot tracks and the opening of the Atlantic and Indian Oceans, in *The Sea*, vol. 7, edited by C. Emiliani, pp. 443–487, John Wiley, New York, 1981.

Myhre, A. M., Marine geophysical studies in the Norwegian-Greenland Sea and adjacent margins, doctor of science thesis, Univ. of Oslo, Norway, 1984.

Myhre, A. M., and O. Eldholm, The western Svalbard margin (74°–80°N), *Mar. Pet. Geol.*, *5*, 134–156, 1987.

Myhre, A. M., O. Eldholm, and E. Sundvor, The margin between the Senja and Spitsbergen fracture zones: Implications from plate tectonics, *Tectonophysics*, *89*, 33–50, 1982.

Nunns, A. G., Marine geophysical investigations in the Norwegian-Greenland Sea between the latitudes of 62°N and 74°N, Ph.D. thesis, Univ. of Durham, Durham, England, 1980.

Nunns, A. G., The structure and evolution of the Jan Mayen ridge and surrounding areas, *AAPG Mem.*, *34*, 193–208, 1982.

Nunns, A. G., Plate tectonic evolution of the Greenland-Scotland Ridge and surrounding regions, in *Structure and Development of the Greenland-Scotland Ridge, New Methods and Concepts*, edited by Bott et al., pp. 11–30, Plenum, New York, 1983.

Nunns, A. G., and J. H. Peacock, Correlation, identification and inversion of magnetic anomalies in the Norway Basin, *Earth Evol. Sci.*, *2*, 130–138, 1983.

Perry, R. K., H. S. Fleming, N. Z. Cherkis, R. H. Feden, and P. R. Vogt, Bathymetry of the Norwegian-Greenland and Western Barents Seas, map, Naval Res. Lab., Washington, D. C., 1980.

Perry, R. K., et al., Bathymetry of the Arctic Ocean, map, Nav. Res. Lab., Washington, D. C., 1985.

Stein, S., H. J. Melosh, and J. B. Minster, Ridge migration and asymmetric sea-floor spreading, *Earth Planet. Sci. Lett.*, *36*, 51–62, 1977.

Sundvor, E., O. Eldholm, A. Gidskehaug, and A. M. Myhre, Marine geophysical survey on the western and northern continental margin off Svalbard, *Sci. Rep. 4*, 35 pp., Univ. of Bergen, Seismol. Obs., 1977.

Talwani, M., and O. Eldholm, Evolution of the Norwegian-Greenland Sea, *Geol. Soc. Am. Bull.*, *88*, 969–999, 1977.

Thiede, J., S. Pfirman, H.-W. Schenke, and W. Reil, Bathymetry of the Molloy Deep: Fram Strait between Greenland and Svalbard, *Mar. Geophys. Res.*, *12*, 197–214, 1990.

Vogt, P. R., Geophysical and geochemical signatures and plate tectonics, in *The Nordic Seas*, edited by B. G. Hurdle, Springer-Verlag, New York, 1986.

Vogt, P. R., and O. E. Avery, Tectonic history of the Arctic basins: Partial solutions and unsolved mysteries, in *Marine Geology and Oceanography of the Arctic Seas*, edited by Y. Herman, pp. 83–117, Springer-Verlag, New York, 1974.

Vogt, P. R., R. H. Feden, O. Eldholm, and E. Sundvor, The ocean crust west and north of the Svalbard Archipelago: Synthesis and review of new results, *Polarforschung*, *48*, 1–19, 1978.

Vogt, P. R., R. K. Perry, R. H. Feden, H. S. Fleming, and N. Z. Cherkis, The Greenland-Norwegian Sea and Iceland environment: Geology and geophysics, in *The Ocean Basins and Margins*, vol. 5, *The Arctic Ocean*, edited by A. E. M. Nairn and M. Churkin, pp. 493–598, Plenum, New York, 1981.

Vogt, P. R., L. C. Kovacs, L. C. Bernero, and S. P. Srivastava, Asymmetric geophysical signatures in the Greenland-Norwegian and Southern Labrador Seas and the Eurasia Basin, *Tectonophysics*, *89*, 95–160, 1982.

Wernicke, B., Low-angle normal faults in the Basin and Range province—Nappe tectonics in an extending orogen, *Nature*, *291*, 645–648, 1981.

Wernicke, B., Uniform-sense normal simple shear of the continental lithosphere, *Can. J. Earth Sci.*, *22*, 108–125, 1985.

Wernicke, B., and B. C. Burchfield, Modes of extensional tectonics, *J. Struct. Geol.*, *4*(2), 105–115, 1982.

R. Buck, Lamont-Doherty Geological Observatory, Palisades, New York, NY 10964.

K. Crane, Department of Geology and Geophysics, Hunter College, 695 Park Avenue, New York, NY 10021.

F. Martinez, Hawaii Institute of Geophysics, University of Hawaii, Honolulu, HA 96822.

E. Sundvor, Seismological Observatory, University of Bergen, Allegaten 41, 5000 Bergen, Norway.

(Received May 2, 1990;
revised April 8, 1991;
accepted April 27, 1991.)